comptes rendus palevol

2026 • 25 • 5

Comparative analysis of the enamel-dentine junction of the lower molars among late Middle Stone Age hominins from northwestern Africa

Hajar ALICHANE, Philipp GUNZ, Robert M. G. MARTIN, Hélène COQUEUGNIOT, Mohamed EL HAJRAOUI, Gregorio OXILIA & Jean-Jacques HUBLIN

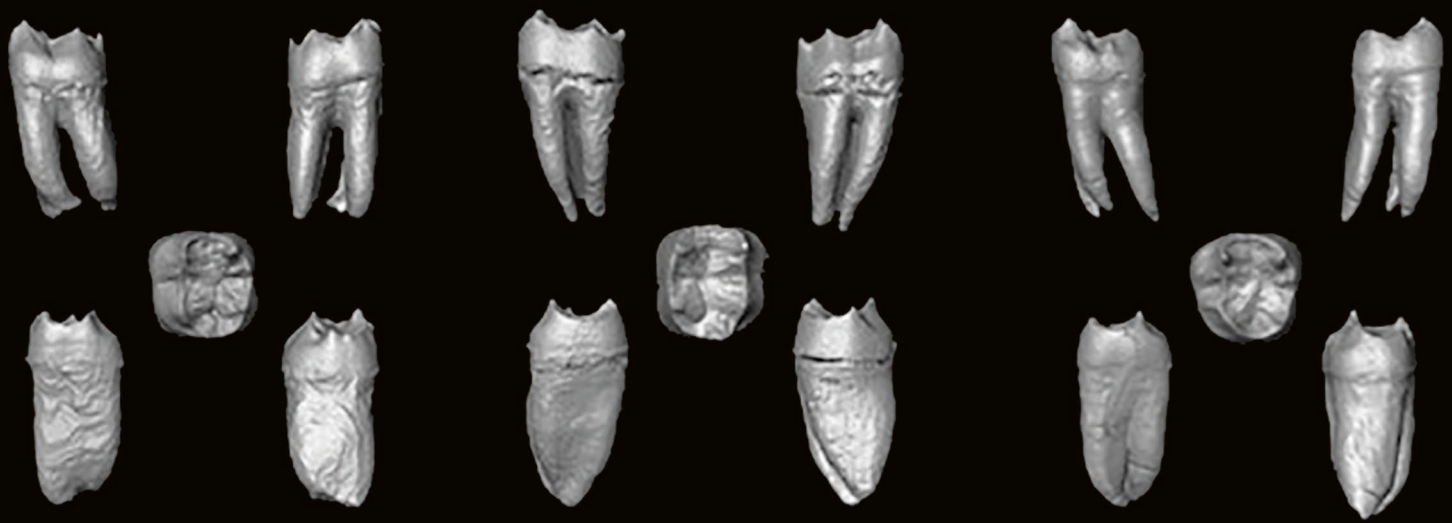

LUCY'S HEIRS – TRIBUTE TO YVES COPPENS

Edited by Jean-Jacques HUBLIN, Aurélien MOUNIER & Nicolas TEYSSANDIER

art. 25 (5) — Published on 18 March 2026
www.cr-palevol.fr

PUBLICATIONS SCIENTIFIQUES

MUSÉUM NAL HIST NATURELLE

Couverture / *Cover* :
Made from the Figures of the article.

Comptes Rendus Palevol est indexé dans / Comptes Rendus Palevol *is indexed by:*
– Cambridge Scientific Abstracts
– Current Contents® Physical
– Chemical, and Earth Sciences®
– ISI Alerting Services®
– Geoabstracts, Geobase, Georef, Inspec, Pascal
– Science Citation Index®, Science Citation Index Expanded®
– Scopus®.

Les articles ainsi que les nouveautés nomenclaturales publiés dans *Comptes Rendus Palevol* sont référencés par / *Articles and nomenclatural novelties published in* Comptes Rendus Palevol *are registered on:*
– ZooBank® (http://zoobank.org)

Comptes Rendus Palevol est une revue en flux continu publiée par les Publications scientifiques du Muséum, Paris et l'Académie des sciences, Paris
Comptes Rendus Palevol *is a fast track journal published by the Museum Science Press, Paris and the Académie des sciences, Paris*

Les Publications scientifiques du Muséum publient aussi / *The Museum Science Press also publish:*
Adansonia, ***Geodiversitas***, ***Zoosystema***, ***Anthropozoologica***, ***European Journal of Taxonomy***, ***Naturae***, ***Cryptogamie*** **sous-sections** ***Algologie***, ***Bryologie***, ***Mycologie***.

L'Académie des sciences publie aussi / *The Académie des sciences also publishes:*
Comptes Rendus Mathématique, ***Comptes Rendus Physique***, ***Comptes Rendus Mécanique***, ***Comptes Rendus Chimie***, ***Comptes Rendus Géoscience***, ***Comptes Rendus Biologies***.

Diffusion – Publications scientifiques Muséum national d'Histoire naturelle
CP 41 – 57 rue Cuvier F-75231 Paris cedex 05 (France)
Tél. : 33 (0)1 40 79 48 05 / Fax : 33 (0)1 40 79 38 40
diff.pub@mnhn.fr / https://sciencepress.mnhn.fr

Académie des sciences, Institut de France, 23 quai de Conti, 75006 Paris.

ISSN (imprimé / *print*) : 1631-0683/ ISSN (électronique / *electronic*) : 1777-571X

Comparative analysis of the enamel-dentine junction of the lower molars among late Middle Stone Age hominins from northwestern Africa

Hajar ALICHANE
École Pratique des Hautes Études (EPHE), Université Paris Sciences & Lettres (PSL),
4-14 rue Ferrus, 75014 Paris (France)
and Max Planck Institute for Evolutionary Anthropology,
Deutscher Platz 6, 04103 Leipzig (Germany)
and Chaire de Paléoanthropologie, Centre interdisciplinaire de recherche en biologie (CIRB),
Collège de France, Université Paris Sciences & Lettres (PSL),
CNRS, 11 place Marcelin Berthelot, 75005 Paris (France)
hajar-alichane@hotmail.com (corresponding author)

Philipp GUNZ
Max Planck Institute for Evolutionary Anthropology,
Deutscher Platz 6, 04103 Leipzig (Germany)
gunz@eva.mpg.de

Robert M. G. MARTIN
Department of Anthropology, University of Toronto,
19 Ursula Franklin Street, Toronto M5S 2S2 (Canada)
rob.martin@mail.utoronto.ca

Hélène COQUEUGNIOT
Archéosciences-Bordeaux, Maison de l'archéologie,
Université Bordeaux Montaigne, Esplanade des Antilles, 33607 Pessac cedex (France)
and École Pratique des Hautes Études (EPHE), Université Paris Sciences & Lettres (PSL),
4-14 rue Ferrus, 75014 Paris (France)
helene.coqueugniot@u-bordeaux-montaigne.fr

Mohamed EL HAJRAOUI
Institut National des Sciences de l'Archéologie et du Patrimoine,
Avenue Allal El-Fassi Hay Riad, BP 6828 Rabat (Morocco)
maelhajraoui@gmail.com

Gregorio OXILIA
Department of Medicine and Surgery, Libera Università Mediterranea (LUM)
University Giuseppe Degennaro, SS 100, Km 18, 70010 Casamassima (BA) (Italy)
oxilia@lum.it

Jean-Jacques HUBLIN
Chaire de Paléoanthropologie, Centre interdisciplinaire de recherche en biologie (CIRB),
Collège de France, Université Paris Sciences & Lettres (PSL),
CNRS, 11 place Marcelin Berthelot, 75005 Paris (France)
and Max Planck Institute for Evolutionary Anthropology,
Deutscher Platz, 6, 04103 Leipzig (Germany)
jean-jacques.hublin@college-de-france.fr

Submitted on 12 February 2024 | Accepted on 20 October 2025 | Published on 18 March 2026

urn:lsid:zoobank.org:pub:1B7C6C65-5CF1-4AB4-BFD3-CFEF8CB983A3

Alichane H., Gunz P., Martin R. M. G., Coqueugniot H., El Hajraoui M., Oxilia G. & Hublin J.-J. 2026. — Comparative analysis of the enamel-dentine junction of the lower molars among late Middle Stone Age hominins from northwestern Africa, *in* Hublin J.-J., Mounier A. & Teyssandier N. (eds), Lucy's Heirs – Tribute to Yves Coppens. *Comptes Rendus Palevol* 25 (5): 77-98. https://doi.org/10.5852/cr-palevol2026v25a5

ABSTRACT

This study investigates the enamel-dentine junction (EDJ) morphology of the first and second mandibular molars (LM1 and LM2) in late Middle Stone Age (MSA) hominins from northwestern Africa, associated with Aterian technocomplexes. These Aterian specimens are compared with fossil *Homo sapiens* from Jebel Irhoud, Qafzeh, Skhul, and Die Kelders, as well as with large samples of *H. neanderthalensis* and recent *H. sapiens*. By focusing exclusively on the EDJ, this study aims to clarify the evolutionary relationships between Aterians and other hominin groups during the Late Pleistocene. Using micro-computed tomography (micro-CT), we analyzed the EDJ in three dimensions, enabling detailed geometric morphometric comparisons. The results reveal a clear trend of molar size reduction within the *H. sapiens* lineage, as well as a morphological distinction between *H. neanderthalensis* and all forms of *H. sapiens*. Aterians are distinct from all other groups due to the larger size of their dentition. Morphologically, the EDJ of the Aterian sample aligns more closely with the sample of fossil *H. sapiens* than with the sample of *H. neanderthalensis*, particularly in LM1s. LM2s display greater variability, with some specimens, such as El Harhoura LRM2 overlapping the range of variation observed in *H. neanderthalensis*. However, this overlap likely reflects the retention of primitive traits within Aterians, due partially to their geological age and partially to their larger size. Our findings contribute to broader discussions on the morphological diversity and evolutionary pathways of fossil *H. sapiens*. The mosaic of dental traits observed in Aterian hominins is discussed in context of regional variations in the evolutionary trajectories of Late Pleistocene hominin populations.

KEY WORDS
Aterian,
Homo sapiens,
MSA,
mandibular molars,
LM1,
LM2,
MicroCT,
EDJ,
geometric,
morphometrics.

RÉSUMÉ

Analyse comparative de la jonction émail-dentine des molaires inférieures chez les hominines de la fin du Middle Stone Age *du nord-ouest de l'Afrique.*

Cette étude examine la morphologie de la jonction émail-dentine (EDJ) des premières et deuxièmes molaires mandibulaires (LM1 et LM2) chez des hominines du *Middle Stone Age* (MSA) tardif en Afrique du Nord-Ouest, associés aux technocomplexes Atériens. Les spécimens atériens sont comparés à ceux d'*Homo sapiens* fossiles provenant de Jebel Irhoud, Qafzeh, Skhul et Die Kelders, ainsi qu'à de larges échantillons d'*H. neanderthalensis* et d'*H. sapiens* récents. En se concentrant exclusivement sur l'EDJ, une région anatomique clé qui conserve des informations sur la forme et la taille, cette étude vise à éclairer les relations évolutives entre les Atériens et d'autres groupes d'Hominines durant le Pléistocène supérieur. À l'aide de la tomodensitométrie à haute résolution (micro-CT), nous avons reconstruit l'EDJ en trois dimensions, permettant des comparaisons morphométriques géométriques détaillées. Les résultats révèlent une tendance marquée à la réduction de la taille des molaires au sein de la lignée des *H. sapiens*, ainsi qu'une distinction morphologique claire entre *H. neanderthalensis* et les différentes formes d'*H. sapiens*. Les spécimens Atériens se distinguent par la taille plus importante de leur dentition par rapport aux autres groupes. Morphologiquement, l'EDJ des Atériens s'aligne davantage avec celle des *H. sapiens* fossiles, notamment pour les LM1, tandis que les LM2 montrent une variabilité accrue ; certains spécimens, tels qu'El Harhoura LRM2, chevauchent le domaine de variation des *H. neanderthalensis*. Ce chevauchement pourrait refléter la rétention de traits primitifs au sein de la population atérienne, attribuable à leur ancienneté géologique et à leur plus grande taille. Nos résultats apportent une contribution significative aux discussions plus larges sur la diversité morphologique et les trajectoires évolutives des *H. sapiens* fossiles. Le caractère mosaïque des traits dentaires observés chez les Hominines Atériens est analysé à la lumière des variations régionales dans les trajectoires évolutives des populations d'Hominines du Pléistocène supérieur.

MOTS CLÉS
Atérien,
Homo sapiens,
MSA,
molaires mandibulaires,
LM1,
LM2,
MicroCT,
EDJ,
géométriques,
morphométriques.

INTRODUCTION

North Africa has yielded a rich Middle/Late Pleistocene fossil record of hominins associated with the Acheulean, Middle Stone Age (MSA), and Iberomaurusian archaeological assemblages. Within the MSA, there is a significant chronological gap between the earliest representatives of *Homo sapiens* in North Africa, dated to approximately 300 ka (Hublin *et al.* 2017; Richter *et al.* 2017), and the hominins associated with late MSA assemblages, spanning a period

of 145 000 years from 160 000 years BP (Bouzouggar *et al.* 2018). This later period provides a substantial fossil record documented across multiple sites.

In this study, we focus on fossils from Morocco associated with late MSA assemblages traditionally assigned to the Aterian technocomplex. The Aterian technocomplex is primarily defined by the presence of pedunculated pieces as "fossiles directeurs", in contrast to older MSA assemblages in the same region, where they are absent (Balout 1955; Tixier 1967; Morel & Le Bretagne 1978; Aumassip 2004). Here, we use "Aterian" to refer to the late MSA in North Africa.

The first Aterian hominin fossil was discovered by Howe and Movius in 1939 at the Mugharet el'Aliya cave in northern Morocco (Şenyürek 1940). In 1951, J. Roche discovered a fragmentary human parietal bone in northern Morocco at the Taforalt Cave, near Oujda, and assigned it to the Aterian technocomplex. Subsequently, in the 1960s and 1970s, additional human fossils associated with Aterian artifacts were unearthed at various sites along the Atlantic coast south of Rabat.

The Rabat-Témara coastal region holds significant archaeological importance and plays a central role in understanding the prehistoric populations of North Africa from the MSA to the Neolithic period. Scholars have been researching this area since the early 20th century, focusing on seven main sites that have yielded Aterian assemblages. These sites span approximately 9 km along the Atlantic coast and have been the subject of research and excavation for over 40 years. Three of these sites, namely the Contrebandiers Cave, El Harhoura I, and Dar es-Soltane II, have produced Pleistocene hominins included in this study.

The Contrebandiers Cave in Témara was first discovered in 1955 by J. Roche, who conducted initial surveys from 1955 to 1957. Situated approximately 17 km from Rabat, on the left side of the Rabat-Casablanca coastal road, the cave is located about 250 m from the coastline. J. Roche continued excavations at the site between 1967 and 1975, unearthing additional material associated with Aterian tools. From 1975 onwards, J.-P. Texier also contributed to excavation efforts (Roche & Texier 1976). In 1994, Bouzouggar reviewed the stratigraphic sections and resumed limited-scale excavations. Systematic excavations were carried out in 2005 by M.A. El Hajraoui and H.L. Dibble. The Contrebandiers Cave yielded several MSA human fossils. The mandible included in this study was discovered in 1956 by J. Roche, who later also unearthed the posterior portion of a skull.

In 2009, an immature individual represented by a skull, mandible, and some post-cranial elements was discovered by Dibble and El Hajraoui in layer 5 of the cave. The precise context of the adult mandible's discovery is difficult to establish (Vallois & Roche 1958; Roche 1976; Roche & Texier 1976), but it was likely recovered from layer 9 of the MSA series, which has been optically stimulated luminescence (OSL)-dated to 111-92 thousand years before present (BP) (Dibble *et al.* 2012).

Dar es-Soltane II cave is situated on an ancient coastal cliff measuring 6 to 8 meters in height and is currently located approximately 300 meters from the present shoreline. The site was excavated by A. Debénath between 1969 and 1980. During the 1975 excavation campaign, Aterian human remains were discovered in the lower levels of the cave. These Aterian fossils include a partial adult skull, a left hemimandible, and a child's calvaria (Debénath 1976; Raynal & Occhietti 2012). They were found in an archaeologically sterile layer (layer 7) overlain by Aterian deposits. Amino acid racemization dating on associated mollusk shells indicates a maximum age of 85-75 ka BP (Raynal & Occhietti 2012), though an age beyond 100 ka has been proposed based on OSL results (Schwenninger *et al.* 2010). Ferembach (1976) assigned the human remains of Dar es-Soltane II to *Homo sapiens*.

The El Harhoura I cave was discovered by A. Debénath and F.Z. Sbihi-Alaoui in 1977 (Nespoulet & El Hajraoui 2012) and yielded a mandible and an isolated canine during excavation in the same year (Debénath 1980). The age of the specimen remains a topic of controversy. A thermoluminescence date obtained on burnt sandstone from a layer immediately below that of the mandible suggests an age of only 32 150 ± 4 800 years BP (Debénath *et al.* 1986), which is out of the range of the Aterian time span. However, Bergmann *et al.* (2022) mention an unpublished uranium-thorium date from a layer capping the one containing the mandible, which would imply a minimum age of approximately 66 000 BP for the fossil. If this older age is confirmed, it would be more consistent with the mandible's archaic morphology.

The Aterian fossil hominins were initially regarded as Neanderthal-like (Şenyürek 1940) or attributed to earlier stages of the evolution of the genus *Homo*. A mandible discovered at the Contrebandiers Cave was initially assigned to an Acheulean hominin based on its robust bone structure and tooth size (Vallois & Roche 1958). Ménard (1998, 2002) emphasized its dental volumes, which approximate the dimensions observed in *Homo erectus*. However, it is important to note that the archaeological sequence of the Contrebandiers Cave only includes MSA, Iberomaurusian, and Neolithic layers (Dibble *et al.* 2012).

Subsequently, in the 1970s, newly discovered Aterian remains in Dar es-Soltane II and El Harhoura I were described as anatomically closer to extant humans and attributed to early forms of *H. sapiens*. In 1993, Minugh-Purvis re-examined the Mugharet el'Aliya specimen and rejected its attribution to *H. neanderthalensis* (Minugh-Purvis 1993). From an anatomical perspective, recent studies (Harvati & Hublin 2012; Hublin *et al.* 2012; Bergmann *et al.* 2022; Röding *et al.* 2022)but could be much older (35–90 ka support the notion that Aterian hominins represent early forms of *H. sapiens*. From a behavioral perspective, late MSA sites in North Africa yield abundant evidence of complex technological and symbolic behaviors, including the production of bone tools, perforated shell bead ornaments, and the use of pigments (Morel 1974; El Hajraoui 1994; Vanhaereny *et al.* 2006; Bouzouggar *et al.* 2007; d'Errico *et al.* 2009; Richter *et al.* 2010; Dibble *et al.* 2012; M.A. El Hajraoui *et al.* 2012; M. El Hajraoui *et al.* 2012; Bouzouggar *et al.* 2018; Steele *et al.* 2019; Ichou & Bouzouggar 2020; Sehasseh *et al.* 2021).

While Aterian human fossils are currently only known from Morocco, Aterian lithic assemblages are documented across a wide geographic area, ranging from the Atlantic coast of North Africa to the western desert of Egypt and from the Mediterranean to the southern regions of the modern Sahara. These populations were contemporaneous with the first *H. sapiens* populations found outside of Africa, and given their geographical distribution, they may have played a role as one of the sources for the early peopling of Eurasia by *H. sapiens*.

The aim of this paper is to compare the dental evidence provided by Aterian hominins with that of contemporaneous groups such as European *H. neanderthalensis* and early forms of *H. sapiens* from Africa and southwest Asia to clarify their taxonomical position. Teeth are abundant in the fossil record and have proven to be valuable tools for taxonomic discrimination (e.g., Weidenreich 1937; Robinson 1956; Trinkaus 1978; Johanson & White 1979; Wolpoff 1979; Wood *et al.* 1983; Suwa *et al.* 1994; Bermúdez de Castro *et al.* 1999; Bailey 2006; Martinón-Torres *et al.* 2012). Specifically, this study focuses on analyzing the shape and size of the enamel-dentine junction (EDJ).

The development and arrangement of dental cusps are tightly regulated by genetic factors (Jernvall & Jung 2000; Thesleff 2000, 2006), and the outer enamel surface (OES) is commonly utilized, among others, to assess biomechanics of natural teeth (e.g., Ding *et al.* 2023), stomatognatic asymmetry (e.g., Khalaf *et al.* 2005; Oxilia *et al.* 2018) and taxonomic relationships among hominin groups (Romandini *et al.* 2020; Oxilia *et al.* 2023, 2025). Investigations into the relationship between the EDJ and the OES have revealed that the EDJ plays a primary role in shaping the morphology of the OES (Skinner 2008; Skinner *et al.* 2008b, 2010; Morita *et al.* 2014; Guy *et al.* 2015).

The application of micro-computed tomography (micro-CT) allows for precise reconstruction of the EDJ and high-resolution morphometric quantitative analysis of the internal structures of teeth (e.g., Skinner 2008; Skinner *et al.* 2008b, 2009a). By employing precise quantitative criteria to characterize the topography of these surfaces, such as elevation, inclination, orientation, curvature, and occlusal complexity, significant covariation between EDJ and OES morphologies in primate molars has been demonstrated (Guy *et al.* 2013, 2015). Notably, the EDJ is less affected by tooth wear compared to the OES and exhibits a more conservative and ancestral morphology (Butler 1956; Korenhof 1961). Consequently, investigations of the EDJ provide valuable insights into developmental processes (Korenhof 1961) and offer a means to address taxonomic and phylogenetic inquiries (e.g., Corruccini 1987, 1998; Macchiarelli *et al.* 2006; Skinner *et al.* 2008a, b, 2009a, b, 2010; Braga *et al.* 2010; Skinner & Gunz 2010; Bailey *et al.* 2011; Ortiz *et al.* 2012; Zanolli *et al.* 2012, 2014, 2015; Zanolli & Mazurier 2013; Martinón-Torres *et al.* 2014; Martínez de Pinillos *et al.* 2014; Zanolli 2015; Martin *et al.* 2017; Ortiz *et al.* 2017).

Studies focusing on the EDJ have successfully discriminated between primate and hominin fossil species and have also differentiated molars within the same jaw arch arch (e.g., Skinner *et al.* 2008a, 2009a, b).

MATERIAL AND METHODS

Material

In addition to the Aterian specimens (n = 7), our comparative sample includes 98 permanent first and second mandibular molars (LM2 and LM2) attributed to fossil *Homo sapiens* (n = 15), *H. neanderthalensis* (n = 37), and recent *H. sapiens* (n = 47), representing a broad range of chronological and geographical origins (Table 1). The Aterian molars (Fig. 1), which come from Middle Stone Age (MSA) contexts in North Africa, were excavated from key archaeological sites such as Dar es-Soltane II, El Harhoura, and Contrebandiers Cave. These specimens provide valuable insights into the dental morphology of populations associated with the Aterian technocomplex.

The fossil *H. sapiens* molars in our sample range in age from Marine Isotope Stages (MIS) 9 to 4 and originate from sites in North Africa, South Africa, and southwestern Asia. These fossil *H. sapiens* serve as an important comparative group for understanding the evolutionary relationships and dental variation in Aterians.

The *H. neanderthalensis* sample includes specimens dating from approximately 230 to 40 ka, notably individuals from Krapina (Croatia) and Scladina (Belgium), as described in Martin *et al.* (2017).

The recent *H. sapiens* sample consists of individuals from Holocene archaeological sites in Belgium, along with specimens from anatomical collections and clinical dental extractions. In the case of antimeric teeth, only the best-preserved side was considered. Due to the lack of sex data for most fossil specimens, the recent *H. sapiens* sample was not divided by sex.

Methods

The molars in this study were scanned using micro-computed tomography (micro-CT) at the Max Planck Institute for Evolutionary Anthropology in Leipzig, Germany. Scanning was performed with either a BIR ACTIS 225/300 industrial microscanner (130 kV, 100 µA, brass filter 0.25 or 0.50 mm) or a SkyScan 1 172 microscanner (100 kV, 94 µA, aluminum and copper filter 0.5 + 0.04 mm), producing voxel sizes ranging from 15 to 50 µm. To enhance the clarity of the images, a three-dimensional median filter with a core size of either one or three was applied, followed by a medium variance filter of the same size. This filtering protocol was designed to standardize grey levels across tissue regions, improving the differentiation between enamel and dentine while preserving the structural integrity of the EDJ (Skinner 2008; Wollny *et al.* 2013).

Enamel and dentine were segmented using Avizo 9.0.1, based on 3D voxel value histograms and grayscale thresholds, and the EDJ surface was generated with unconstrained smoothing. All analyses were conducted exclusively on the EDJ (Fig. 2). In certain specimens, such as the Contrebandiers Mandible LLM1, Dar es-Soltane II H4 LLM1, and El Harhoura LRM1, dental wear compromised the dentine horn tips. For these teeth, the original height and position of the cusp tips were estimated using a prediction pipeline (Napolitano *et al.* 2026). The predicted heights were applied

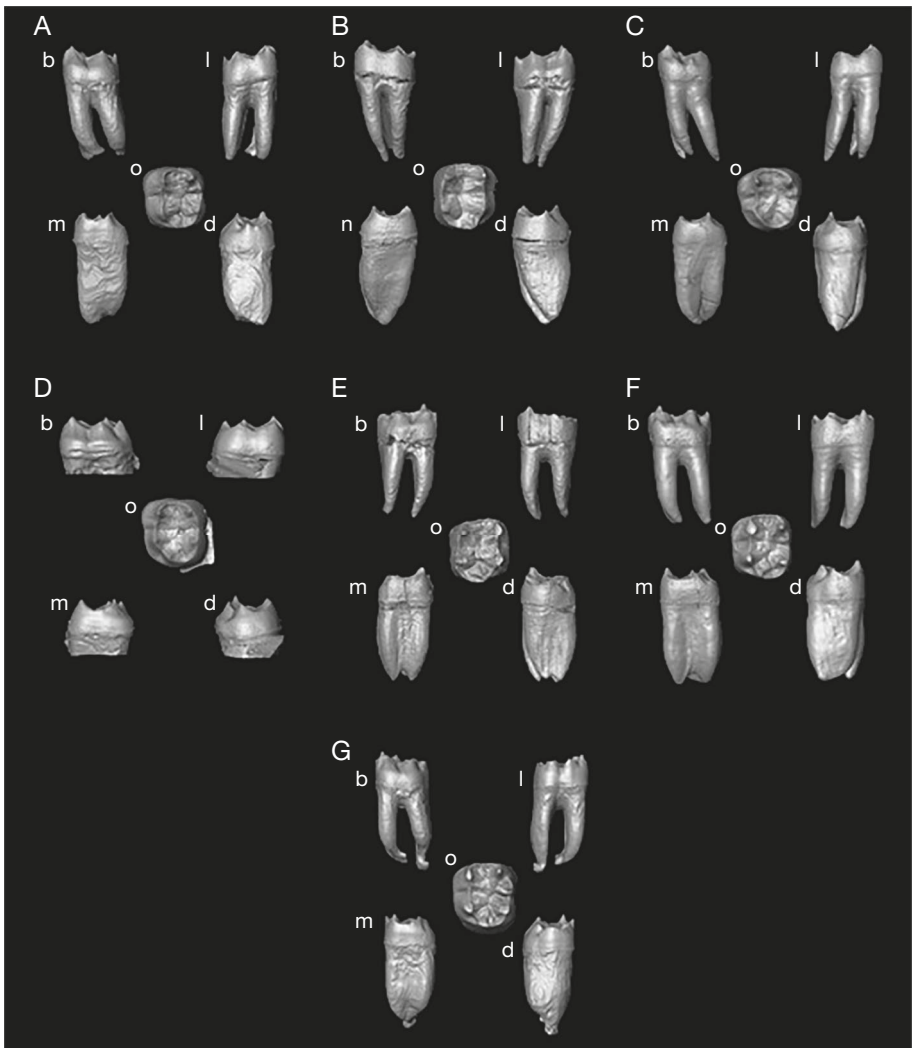

Fig. 1. — 3D digital model of the dentine and enamel-dentine junction (EDJ) of the Aterian specimens: **A**, Dar es-Soltane II H4 LLM2; **B**, El Harhoura LRM2; **C**, Contrebandiers Mandible LLM2; **D**, Contrebandiers Mandible T3a LLM1; **E**, El Harhoura LRM1; **F**, Contrebandiers Mandible LLM1; **G**, Dar es-Soltane II H4 LRM1. Abbreviations: **b**, buccal; **d**, distal; **l**, lingual; **m**, mesial; **o**, occlusal.

to the digital models at positions defined as the midpoints between two reference points located mesially and distally to the wear margin, a method shown to accurately reflect the original cusp position.

The original cusp heights for the three worn Aterian molars (Fig. 3) – Dar es-Soltane II H4 LLM1, El Harhoura LRM_1, and Contrebandiers Mandible LLM1 – were estimated using a standardized machine learning pipeline specifically designed for the reconstruction of original cusp morphology in worn mandibular molars (Napolitano *et al.* 2026). This approach relies on three-dimensional morphometric data derived from micro-computed tomography (micro-CT) and integrates both Random Forest regression and ensemble modeling strategies. The reference dataset used for model development consisted of 40 unworn permanent mandibular molars (19 M1 and 21 M2), spanning four hominin groups (Middle Paleolithic *Homo sapiens*, recent *Homo sapiens*, Neanderthals, and modern individuals). The teeth were scanned at voxel resolutions between 15-50 µm and subsequently pre-processed to optimize image clarity (median and variance filters, beam-hardening and ring correction) and segmentation accuracy, with enamel, dentine, and pulp chamber reconstructed as separate volumes. The EDJ, which preserves morphogenetic information even in worn teeth, was extracted and used as the primary structural reference. To model variation induced by wear, two digital simulations of progressive occlusal attrition ("worn1" and "worn2") were generated for each tooth, yielding a total of 120 experimental observations. For each state, cusp-specific morphometric variables (area and volume) were quantified, while the original cusp height served as the predictive target variable. Regression models (Random Forest and linear regression) were trained on unworn specimens and validated on simulated worn specimens via a hold-out strategy, with root mean square error (RMSE) and R^2 as performance metrics. Species identity was deliberately excluded as a predictor to maximize model generalizability across morphological diversity. The Random Forest model consistently outperformed

TABLE 1. — Fossil and extant specimens included in this study.

Group	Chronology	Source for chronology	Locality	Tooth position
Aterian				
	MIS 5	Barton *et al.* 2009	Dar es-Soltane II, Morocco	LLM1
	MIS 5	Barton *et al.* 2009	Dar es-Soltane II, Morocco	LLM2
	MIS 5	Schwenninger *et al.* 2010	El Harhoura, Morocco	LRM1
	MIS 5	Schwenninger *et al.* 2010	El Harhoura, Morocco	LRM2
	MIS 5	Jacobs *et al.* 2011	Contrebandiers, Morocco	LLM1
	MIS 5	Jacobs *et al.* 2011	Contrebandiers, Morocco	LLM2
	MIS 5	Jacobs *et al.* 2011	Contrebandiers, Morocco	LLM1
Fossil *Homo sapiens*				
	MIS 5	Schwarcz & Rink 2000	Die Kelders, South Africa	LRM1
	MIS 5	Schwarcz & Rink 2000	Die Kelders, South Africa	LLM1
	MIS 5	Schwarcz & Rink 2000	Die Kelders, South Africa	LRM2
	MIS 5	Grine & Klein 1985	Equus, South Africa	LRM1
	MIS 8-9	Richter *et al.* 2017	Irhoud, Morocco	LRM2
	MIS 8-9	Richter *et al.* 2017	Irhoud, Morocco	LRM1
	MIS 8-9	Richter *et al.* 2017	Irhoud, Morocco	LLM2
	MIS 5	Mercier *et al.* 1993; Valladas *et al.* 1988	Qafzeh, Israel	LLM1
	MIS 5	Mercier *et al.* 1993; Valladas *et al.* 1988	Qafzeh, Israel	LLM2
	MIS 5	Mercier *et al.* 1993; Valladas *et al.* 1988	Qafzeh, Israel	LLM1
	MIS 5	Mercier *et al.* 1993; Valladas *et al.* 1988	Qafzeh, Israel	LLM2
	MIS 5	Mercier *et al.* 1993; Valladas *et al.* 1988	Qafzeh, Israel	LLM2
	MIS 5	Mercier *et al.* 1993; Valladas *et al.* 1988	Qafzeh, Israel	LLM1
	MIS 5	Mercier *et al.* 1993; Valladas *et al.* 1988	Qafzeh, Israel	LRM2
	MIS 5	Mercier *et al.* 1993; Valladas *et al.* 1988	Skhul, Israel	LLM1
Homo neanderthalensis				
	MIS 6	Teilhol 2002	Abri Suard, France	LRM1
	MIS 6	Teilhol 2002	Abri Suard, France	LRM1
	MIS 6	Teilhol 2002	Abri Suard, France	LLM1
	MIS 6	Teilhol 2002	Abri Suard, France	LLM2
	MIS 5a-4	Guadelli & Laville 1988	Combe-Grenal, France	LRM1
	MIS 5a-4	Guadelli & Laville 1988	Combe-Grenal, France	LLM1
	MIS 5a-4	Guadelli & Laville 1988	Combe-Grenal, France	LRM1
	MIS 5e	Rink *et al.* 1995	Krapina, Croatia	LLM2
	MIS 5e	Rink *et al.* 1995	Krapina, Croatia	LLM2
	MIS 5e	Rink *et al.* 1995	Krapina, Croatia	LRM2
	MIS 5e	Rink *et al.* 1995	Krapina, Croatia	LLM1
	MIS 5e	Rink *et al.* 1995	Krapina, Croatia	LRM1
	MIS 5e	Rink *et al.* 1995	Krapina, Croatia	LRM2
	MIS 5e	Rink *et al.* 1995	Krapina, Croatia	LLM1
	MIS 5e	Rink *et al.* 1995	Krapina, Croatia	LLM2
	MIS 5e	Rink *et al.* 1995	Krapina, Croatia	LLM1
	MIS 5e	Rink *et al.* 1995	Krapina, Croatia	LLM2
	MIS 5e	Rink *et al.* 1995	Krapina, Croatia	LRM2
	MIS 5e	Rink *et al.* 1995	Krapina, Croatia	LRM2
	MIS 5e	Rink *et al.* 1995	Krapina, Croatia	LLM2
	MIS 5e	Rink *et al.* 1995	Krapina, Croatia	LRM1
	MIS 5e	Rink *et al.* 1995	Krapina, Croatia	LRM2
	MIS 5e	Rink *et al.* 1995	Krapina, Croatia	LLM1
	MIS 5e	Rink *et al.* 1995	Krapina, Croatia	LLM2
	MIS 5e	Rink *et al.* 1995	Krapina, Croatia	LLM2
	MIS 4-3	Martin 1920; Mercier 1992; Mercier & Valladas 1998	La Quina France	LLM2
	MIS 3	Mellars & Grün 1991; Valladas *et al.* 1986	Le Moustier, France	LLM1
	MIS 3	Mellars & Grün 1991; Valladas *et al.* 1986	Le Moustier, France	LLM2
	MIS 5c-4	Cavanhié 2011; Delpech 1996; Turq *et al.* 2008; Vandermeersch & Trinkaus 1995	Regourdou, France	LLM2
	MIS 4	Guérin *et al.* 2012	Roc de Marsal, France	LRM1
	MIS 5c	Ellwood *et al.* 2004; Pirson *et al.* 2014	cladina, Belgium	LRM1
	MIS 5c	Ellwood *et al.* 2004; Pirson *et al.* 2014	Scladina, Belgium	LRM2
	MIS 5c	Ellwood *et al.* 2004; Pirson *et al.* 2014	Scladina, Belgium	LLM2
	MIS 5c	Ellwood *et al.* 2004; Pirson *et al.* 2014	Scladina, Belgium	LRM2
	MIS 5c	Ellwood *et al.* 2004; Pirson *et al.* 2014	Scladina, Belgium	LRM1
	MIS 5c	Ellwood *et al.* 2004; Pirson *et al.* 2014	Scladina, Belgium	LLM1
	MIS 3	Wild *et al.* 2001	Vindija Cave, Croatia	LRM2
Recent *Homo sapiens*				
	MIS 1	–	Archaeological sites in Belgium	LLM1
	MIS 1	–	Archaeological sites in Belgium	LRM2

Table 1. — Continuation.

Group	Chronology	Source for chronology	Locality	Tooth position
	MIS 1	–	Archaeological sites in Belgium	LLM1
	MIS 1	–	Archaeological sites in Belgium	LLM1
	MIS 1	–	Archaeological sites in Belgium	LRM1
	MIS 1	–	Archaeological sites in Belgium	LLM1
	MIS 1	–	Anatomical collections / Clinical extractions	LLM2
	MIS 1	–	Anatomical collections / Clinical extractions	LRM2
	MIS 1	–	Anatomical collections / Clinical extractions	LLM2
	MIS 1	–	Anatomical collections / Clinical extractions	LRM1
	MIS 1	–	Anatomical collections / Clinical extractions	LRM2
	MIS 1	–	Anatomical collections / Clinical extractions	LLM2
	MIS 1	–	Anatomical collections / Clinical extractions	LRM2
	MIS 1	–	Anatomical collections / Clinical extractions	LRM2
	MIS 1	–	Anatomical collections / Clinical extractions	LLM2
	MIS 1	–	Anatomical collections / Clinical extractions	LLM1
	MIS 1	–	Anatomical collections / Clinical extractions	LLM2
	MIS 1	–	Anatomical collections / Clinical extractions	LLM1
	MIS 1	–	Anatomical collections / Clinical extractions	LLM2
	MIS 1	–	Anatomical collections / Clinical extractions	LLM1
	MIS 1	–	Anatomical collections / Clinical extractions	LLM2
	MIS 1	–	Anatomical collections / Clinical extractions	LRM1
	MIS 1	–	Anatomical collections / Clinical extractions	LLM1
	MIS 1	–	Anatomical collections / Clinical extractions	LLM1
	MIS 1	–	Anatomical collections / Clinical extractions	LRM2
	MIS 1	–	Anatomical collections / Clinical extractions	LLM2
	MIS 1	–	Anatomical collections / Clinical extractions	LLM1
	MIS 1	–	Anatomical collections / Clinical extractions	LRM2
	MIS 1	–	Anatomical collections / Clinical extractions	LLM1
	MIS 1	–	Anatomical collections / Clinical extractions	LLM2
	MIS 1	–	Anatomical collections / Clinical extractions	LRM2
	MIS 1	–	Anatomical collections / Clinical extractions	LLM2
	MIS 1	–	Anatomical collections / Clinical extractions	LLM2
	MIS 1	–	Anatomical collections / Clinical extractions	LLM2
	MIS 1	–	Anatomical collections / Clinical extractions	LRM2
	MIS 1	–	Anatomical collections / Clinical extractions	LLM1
	MIS 1	–	Anatomical collections / Clinical extractions	LRM1
	MIS 1	–	Anatomical collections / Clinical extractions	LRM2
	MIS 1	–	Anatomical collections / Clinical extractions	LLM1
	MIS 1	–	Anatomical collections / Clinical extractions	LLM1
	MIS 1	–	Anatomical collections / Clinical extractions	LRM2
	MIS 1	–	Anatomical collections / Clinical extractions	LRM1
	MIS 1	–	Anatomical collections / Clinical extractions	LRM2
	MIS 1	–	Anatomical collections / Clinical extractions	LLM2
	MIS 1	–	Anatomical collections / Clinical extractions	LLM1
	MIS 1	–	Anatomical collections / Clinical extractions	LRM1
	MIS 1	–	Anatomical collections / Clinical extractions	LRM1

TABLE 2. — Summary table of dental cusps analyzed from three individuals (Dar es-Soltane II H4 LLM1, El Harhoura LRM1, Contrebandiers Mandible LLM1), indicating the strategy used, the best predictive model, input area and volume measurements, and the predicted height for each cusp. The predicted height value is calculated from the cutting plane obtained from the occlusal basin, which was derived by applying an offset parallel to the cervical.

Tooth_ID	Cusp	Strategy used	Best model	Area input	Volume input	Predicted height
Dar es-Soltane II H4 LLM1	Protoconid	Uniti	Random forest	23.18	34.84	3.314
Dar es-Soltane II H4 LLM1	Metaconid	Uniti	Ensemble	13.61	20.14	3.708
Dar es-Soltane II H4 LLM1	Entoconid	Uniti	Random forest	15.16	16.53	2.461
Dar es-Soltane II H4 LLM1	Hypoconid	Uniti	Random forest	17.24	20.44	2.323
El Harhoura LRM1	Protoconid	Uniti	Random forest	22.31	33.57	3.04
El Harhoura LRM1	Metaconid	Uniti	Ensemble	22.84	30.94	3.837
El Harhoura LRM1	Entoconid	Uniti	Random forest	16.81	24.56	2.437
El Harhoura LRM1	Hypoconid	Uniti	Random forest	21.46	16.19	2.184
Contrebandiers Mandible LLM1	Protoconid	Uniti	Random forest	20.79	33.89	3.178
Contrebandiers Mandible LLM1	Metaconid	Uniti	Ensemble	23.67	28.2	3.533
Contrebandiers Mandible LLM1	Entoconid	Uniti	Random forest	21.89	13.39	2.447
Contrebandiers Mandible LLM1	Hypoconid	Uniti	Random forest	14.62	28.83	2.904

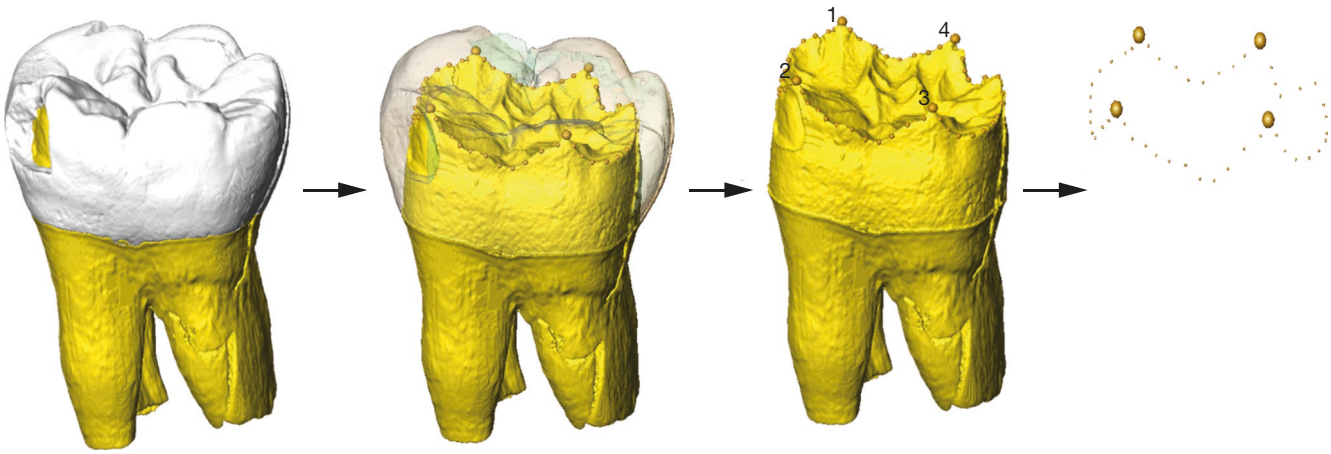

Fig. 2. — Landmarking protocol for mandibular molar Irhoud3 LRM_1 Anatomical landmarks (**big spheres**) are placed on the tips of the four primary horns: **1**, protoconid; **2**, metaconid; **3**, entoconid; **4**, hypoconid. Curve semilandmarks (**small spheres**) are placed along the ridge of the enamel-dentine junction (EDJ).

linear regression, while ensemble predictions provided stable intermediate results. Validation showed strong predictive accuracy across all cusp types (RMSE < 0.25 mm; $R^2 > 0.83$), even under conditions of advanced simulated wear. These results demonstrate that the pipeline offers a robust and reproducible solution for estimating original cusp heights from worn teeth, overcoming the limitations imposed by occlusal attrition. On this basis, the original cusp heights of the Aterian molars reported here were reconstructed from their measured occlusal areas and volumes (Table 2).

For geometric morphometric analysis, two sets of 3D landmarks were collected following established protocols (Skinner 2008; Skinner *et al.* 2008a, 2009a; Skinner & Gunz 2010). Four anatomical landmarks were digitized at the tips of the dentine horns corresponding to the primary cusps (protoconid, metaconid, entoconid, and hypoconid). Additionally, semilandmarks were placed along the EDJ ridges connecting the dentine horns, starting from the protoconid and proceeding towards the metaconid (Fig. 2). The EDJ ridge was divided into four sections, with a predefined number of semilandmarks placed equidistantly within each section: 12 between the protoconid and metaconid, 12 between the metaconid and entoconid, 24 between the entoconid and hypoconid, and 12 between the hypoconid and protoconid. To ensure uniformity in measurement points across all specimens (n = 60), semilandmarks were resampled using a Mathematica routine and subsequently adjusted using a sliding algorithm to minimize thin-plate spline bending energy, thereby aligning each specimen with the Procrustes average shape (Gunz *et al.* 2005; Mitteroecker & Gunz 2013).

Once the sliding was completed, a Procrustes superimposition (Rohlf & Slice 1990) was applied to transform the landmark data into shape coordinates. These Procrustes shape coordinates were subsequently analyzed using multivariate statistics in shape space (Mitteroecker *et al.* 2013), providing a detailed framework for examining shape variation among groups.

Beyond the shape analyses, Procrustes form space was also explored by incorporating both the natural logarithm of centroid size and the Procrustes shape coordinates in a principal component analysis (PCA). This dual approach allowed for the evaluation of both size and shape differences across taxa, adding a further dimension to the analysis.

To statistically assess the differences in centroid size among groups, computations were performed using R software. Separate ANOVA tests were conducted for LM1 and LM2, followed by post hoc Tukey tests.

RESULTS

Reconstruction of worn EDJ

Predicted cusp heights for Dar es-Soltane II H4 LLM1 ranged from 2.32 mm (hypoconid) to 3.71 mm (metaconid), while El Harhoura LRM_1 showed values from 2.18 mm (hypoconid) to 3.84 mm (metaconid). For the Contrebandiers Mandible LLM1, predicted heights ranged from 2.45 mm (entoconid) to 3.53 mm (metaconid).

Subsequently, these predictions were applied on digital models (Fig. 3) and used to optimally calibrate the placement of the cusp landmark for each cusp.

Centroid sizes of LM1 and LM2

The centroid sizes in this study were analyzed to examine the variation in molar sizes across different hominin groups and positions (LM1 and LM2) (Appendices 1; 2). A boxplot in Figure 4 visually represents this variation, where the central line within each box denotes the median, dividing the data into two halves. The edges of the box correspond to the interquartile range (IQR), representing the central 50% of the data. Whiskers extend to capture the upper and lower 25% of the distribution, providing an overview of variability beyond the IQR.

This boxplot comparison allows for a clear visualization of size differences between groups based on molar position and taxonomic classification. Examining the centroid size of the EDJ for LM1 and LM2 across Aterian, fossil *H. sapiens*, *H. neanderthalensis*, and recent *H. sapiens* offers insight into evolutionary trends in molar size.

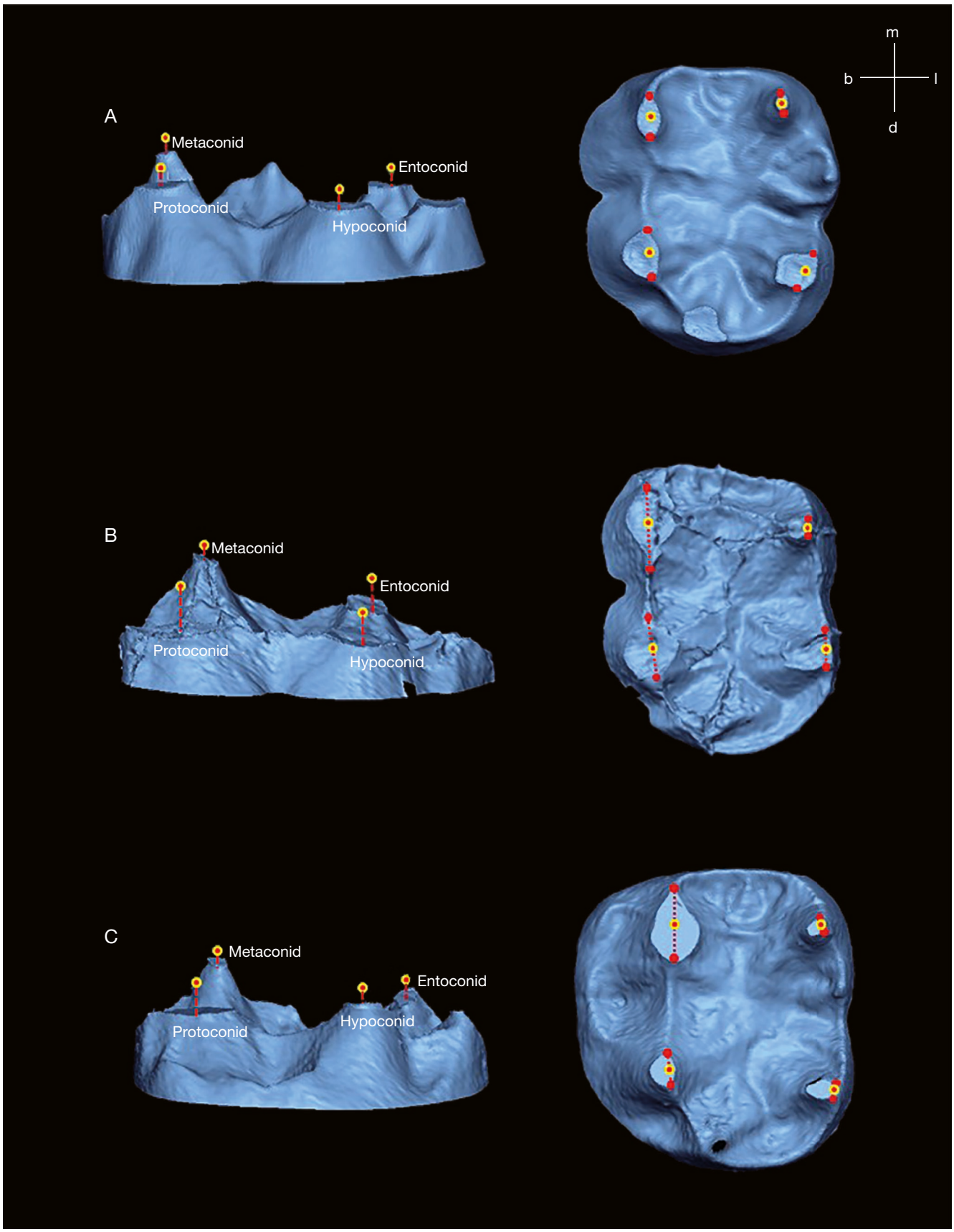

Fig. 3. — Predicted cusp heights for three Aterian molars where severe occlusal wear, extending to the enamel-dentine junction (EDJ), required estimation: **A**, Dar es-Soltane II H4 LLM1; **B**, El Harhoura LRM1; **C**, Contrebandiers Mandible LLM1.

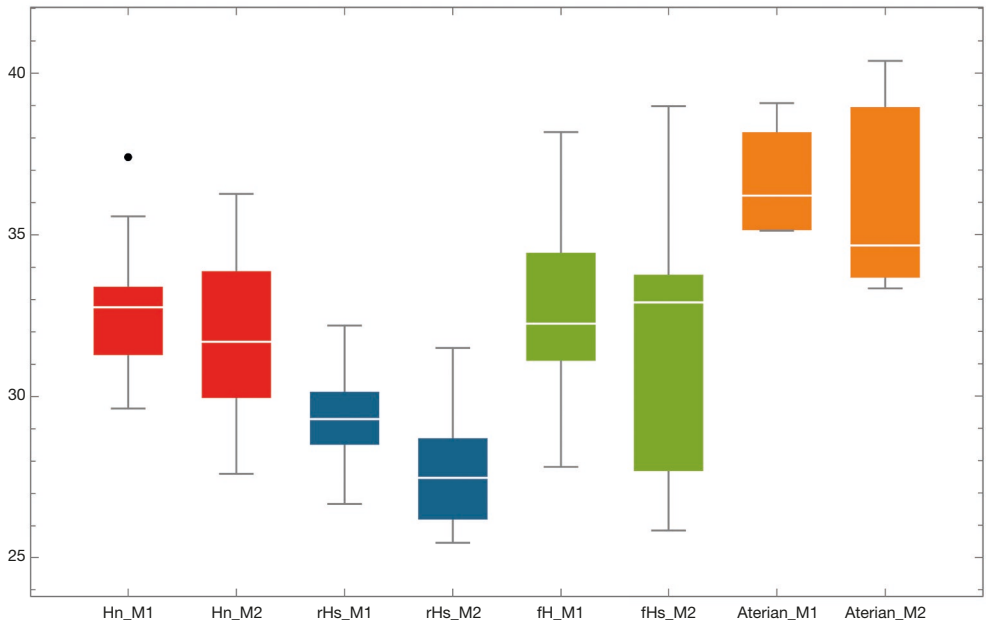

Fig. 4. — Boxplot of the centroid size by molar type LM1 and LM2, across Aterian (**orange**), fossil *Homo sapiens* (**green**), *H. neanderthalensis* (**red**), and recent *H. sapiens* specimens (**blue**). Hn-M1 (n = 17), Hn-M2 (n = 20), RHS-M1 (n = 23), RHS-M2 (n = 24), FHS-M1 (n = 8), FHS-M2 (n = 7), Aterian-M1 (n = 4), Aterian-M2 (n = 3).

Table 3. — Statistical results summary of the first mandibular molars (LM1) across Aterian, fossil *Homo sapiens*, *H. neanderthalensis* and recent *H. sapiens* specimens.

Comparison	Mean difference	p-value (Tukey)	Significance
Fossil *H. sapiens* vs Aterian	–3.95	0.012	Significant
H. neanderthalensis vs Aterian	–4.02	0.003	Significant
Recent *H. sapiens* vs Aterian	–7.33	0	Significant
H. neanderthalensis vs fossil *H. sapiens*	–0.07	1	Not significant
Recent *H. sapiens* vs fossil *H. sapiens*	–3.39	0	Significant
Recent *H. sapiens* vs *H. neanderthalensis*	–3.31	0	Significant

This comparative approach reveals patterns of size evolution across lineages, highlighting distinct size distributions and overlaps among these groups.

LM1 centroid size

For the LM1 centroid size, significant differences are observed across all hominin groups. The Aterian LM1 exhibits the largest centroid size among the groups analyzed, with limited overlap with other groups. This distinctively larger size range suggests that Aterian LM1s maintain unique morphological characteristics, setting them apart from other groups in the study. Statistical analysis further reinforces this observation, indicating a clear separation between the centroid sizes of Aterian LM1s and those of fossil *H. sapiens*, *H. neanderthalensis*, and recent *H. sapiens* (Table 3).

LM2 centroid size

For the LM2 centroid size, the pattern reveals some notable distinctions. Aterian LM2s maintain larger centroid sizes compared to recent *H. sapiens*, whose sizes are distinctly smaller. However, Aterian LM2s show some overlap in centroid size range with both fossil *H. sapiens* and *H. neanderthalensis* (Fig. 3). This overlap, though minimal, may indicate the retention of certain ancestral traits within the Aterian group.

Statistical comparisons confirm that while recent *H. sapiens* show significant differences from Aterians in LM2 centroid size, the differences between Aterians, fossil *H. sapiens*, and *H. neanderthalensis* are not statistically significant. This finding highlights a closer similarity in the LM2 position among these three groups (Table 4).

Principal component analysis of LM1 EDJ shape and form

In the shape space, the PCA of LM1 reveals distinct patterns of morphological variation among Aterian, *H. neanderthalensis*, fossil *H. sapiens*, and recent *H. sapiens* specimens. In the PC1 (19.50% of variance) vs PC2 (14.57% of variance) plot (Fig. 5A), Aterian specimens show a distinct and relatively concentrated clustering compared to the other groups, indicating a unique combination of shape characteristics. Along PC2, Aterians exhibit substantial overlap with fossil and recent

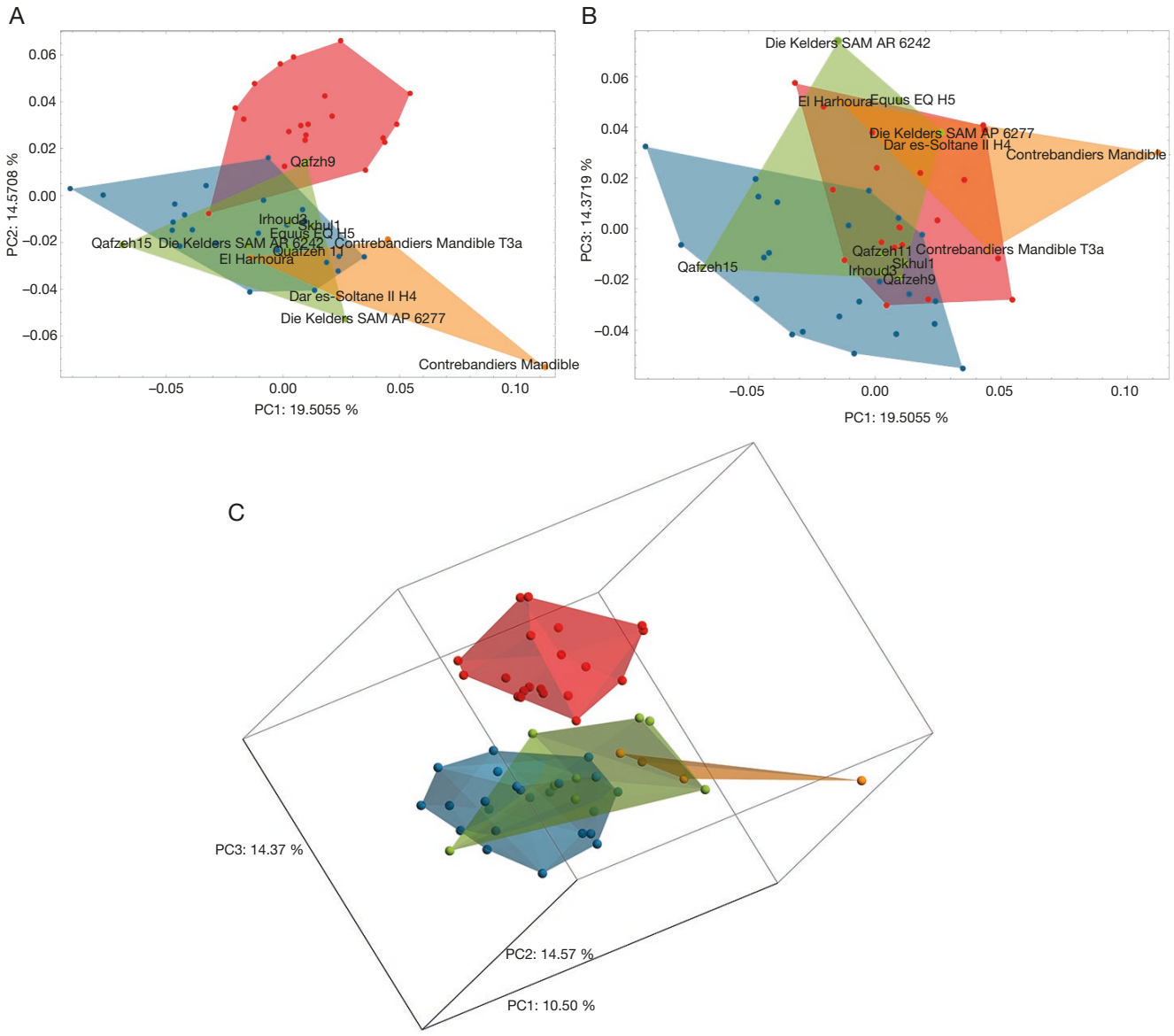

FIG. 5. — Principal component analysis (PCA) plots of enamel-dentine junction (EDJ) shape the first mandibular molar across Aterian (**orange**), fossil *Homo sapiens* (**green**), *H. neanderthalensis* (**red**), and recent *H. sapiens* specimens (**blue**): **A**, first mandibular molars (LM1) EDJ shape (PC1 vs PC2); **B**, LM1 EDJ shape (PC1 vs PC3); **C**, LM1 EDJ shape (PC1, PC2, and PC3).

TABLE 4. — Statistical results summary of the second mandibular molars (LM2) across Aterian, fossil *Homo sapiens*, *H. neanderthalensis* and recent *H. sapiens* specimens.

Comparison	Mean difference	p-value (Tukey)	Significance
Fossil *H. sapiens* vs Aterian	–4.32	0.097	Not significant
H. neanderthalensis vs Aterian	–4.25	0.058	Not significant
Recent *H. sapiens* vs Aterian	–8.50	0	Significant
H. neanderthalensis vs Fossil *H. sapiens*	0.08	1	Not significant
Recent *H. sapiens* vs fossil *H. sapiens*	–4.18	0.003	Significant
Recent *H. sapiens* vs *H. neanderthalensis*	–4.26	0	Significant

H. sapiens, while remaining well-separated from *H. neanderthalensis*. Although Aterians partly overlap with both fossil and recent *H. sapiens*, their distribution is shifted toward higher positive values on PC1, reflecting their larger size.

In the PCA plot comparing PC1 (19.50% of variance) and PC3 (14.37% of variance) (Fig. 5B), Aterian specimens show some overlap with both *H. neanderthalensis* and fossil *H. sapiens*. Contrebandiers T3a LLM1 clusters within the variation observed

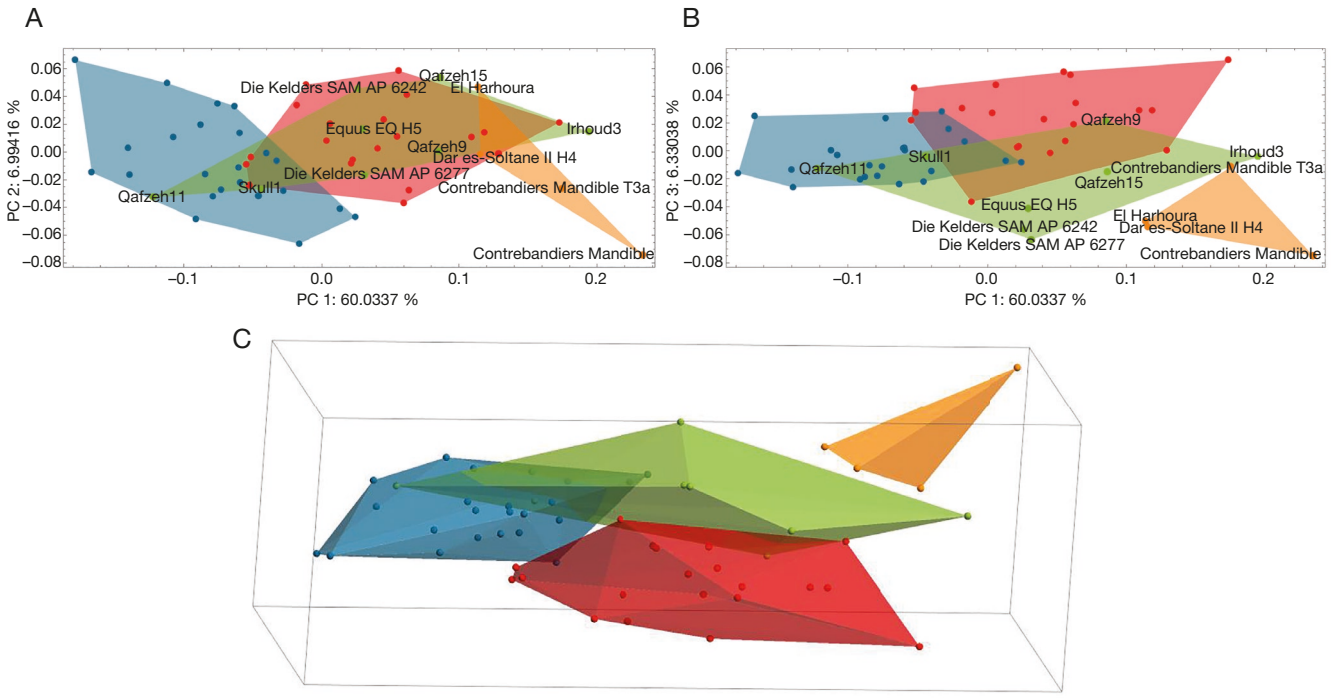

Fig. 6. — Principal component analysis (PCA) plots of enamel-dentine junction (EDJ) form the first mandibular molar across Aterian (**orange**), fossil *Homo sapiens* (**green**), *H. neanderthalensis* (**red**), and recent *H. sapiens* specimens (**blue**): **A**, first mandibular molars (LM1) EDJ form (PC1 vs PC2); **B**, LM1 EDJ shape form (PC1 vs PC3); **C**, LM1 EDJ form (PC1, PC2, and PC3).

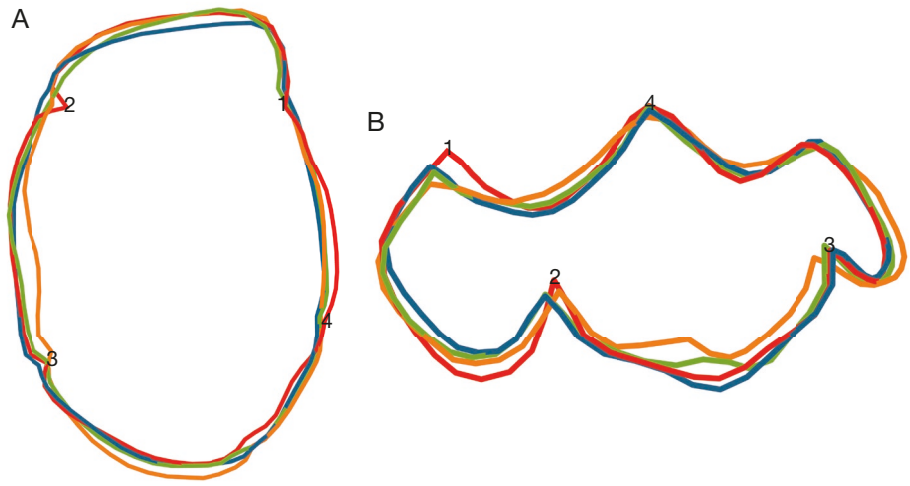

Fig. 7. — Between taxa comparisons of mean enamel-dentine junction (EDJ) shape of first mandibular molars: **A**, first mandibular molars (LM1) occlusal view; **B**, LM1 lateral view, across Aterians (**orange**), fossil *Homo sapiens* (**green**), *H. neanderthalensis* (**red**), and recent *Homo sapiens* (**blue**). Key landmarks: **1**, protoconid; **2**, metaconid; **3**, entoconid; **4**, hypoconid.

for *H. neanderthalensis*, while El Harhoura LRM1 and Dar es-Soltane II H4 LLM1 specimens closely align with both *H. neanderthalensis* and fossil *H. sapiens*. Additionally, El Harhoura appears distinct from all other groups. Certain fossil *H. sapiens* specimens, including Qafzeh 11, Irhoud 3, and Skhul 1, cluster with both *H. neanderthalensis* and recent *H. sapiens*.

A 3D plot of the shape space following PC1, PC2, and PC3 (Fig. 5C) offers a clear depiction of the morphological distinctions among the groups. *Homo neanderthalensis* individuals are completely separated from all other groups, highlighting the uniqueness of their LM1 morphology. Aterian specimens, though more closely clustered with fossil *H. sapiens,* retain distinct characteristics. While there is some marginal overlap with fossil *H. sapiens*, Aterians do not overlap with recent *H. sapiens*. Interestingly, recent *H. sapiens*, fossil *H. sapiens*, and Aterians form a separate cluster along PC2, which is well-distinguished from *H. neanderthalensis*.

In the form space analysis of PC1 vs PC2 (Fig. 6A), PC1 accounts for 60.03% of variance, while PC2 explains 6.99%. Aterian specimens occupy a distinct position with higher

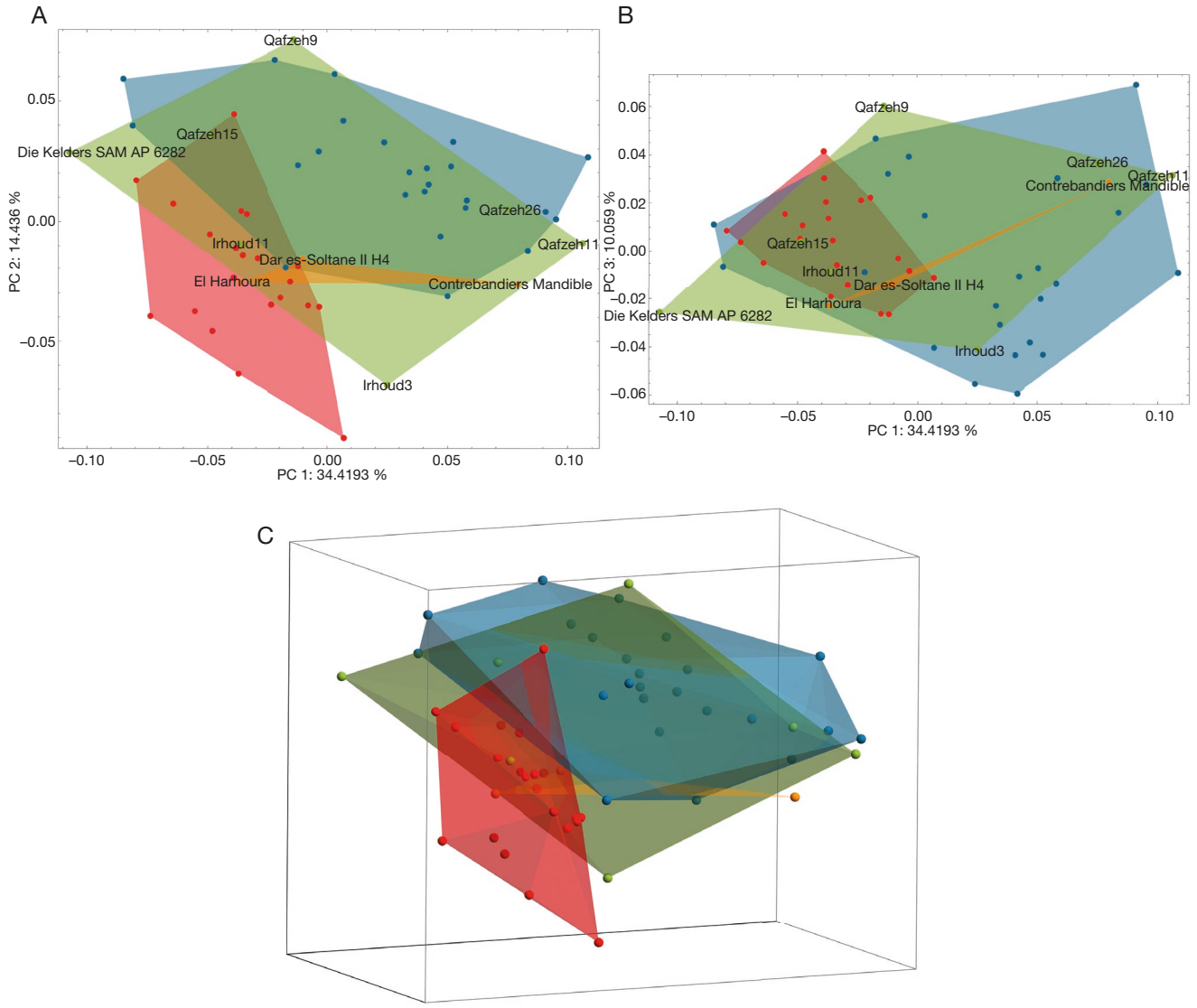

FIG. 8. — Principal component analysis (PCA) plots of enamel-dentine junction (EDJ) shape the second mandibular molar across Aterian (**orange**), fossil *Homo sapiens* (**green**), *H. neanderthalensis* (**red**), and recent *H. sapiens* specimens (**blue**): **A**, second mandibular molars (LM2) EDJ shape (PC1 vs PC2); **B**, LM2 EDJ shape (PC1 vs PC3); **C**, LM2 EDJ shape (PC1, PC2, and PC3).

positive values along PC1. This positioning reflects the larger sizes observed in Aterian LM1s as well as in most *H. neanderthalensis* and fossil *H. sapiens* when compared to recent *H. sapiens*. Fossil *H. sapiens* show the largest variability along PC1, indicating considerable diversity in their molar size.

In PC1 vs PC3 form space (Fig. 6B), PC1 accounts for 60.03% of the total variance, while PC3 explains 6.30%. Aterians are positioned distinctly from both *H. neanderthalensis* and *H. sapiens*. Along PC3, the differences between recent *H. sapiens*, fossil *H. sapiens*, and Aterians appear largely driven by size, which sets the Aterians apart from the others.

In a 3D shape form space (Fig. 6C), the extreme positioning of Aterians becomes even more evident, while the distinctive pattern of *H. neanderthalensis* is clearer. Aterians exhibit a smaller range of variation, likely due to the limited number of available specimens. They position close to the largest fossil *H. sapiens*.

The EDJ shape differences of LM1 (Fig. 7) across Aterians, fossil *H. sapiens*, *H. neanderthalensis*, and recent *H. sapiens* reflect distinct morphological patterns at key cusp landmarks: 1) the protoconid; 2) metaconid; 3) entoconid; and 4) hypoconid.

In the occlusal view of LM1 (Fig. 7A), Aterian molars display an elongated distolingual crest linking the entoconid and hypoconid, which extends distally in an open curve. The crest between the entoconid and hypoconid extends distally in an open curve. Meanwhile, the crest between the entoconid and metaconid is displaced toward the center of the crown. This elongated outline is present, albeit to a lesser extent, in *H. neanderthalensis* and fossil *H. sapiens*.

In recent *H. sapiens*, the EDJ crest outlines are more compact, with shorter and less mesiodistally elongated patterns compared to other groups. In *H. neanderthalensis*, talonid crests are narrower and shorter than those observed in fossil

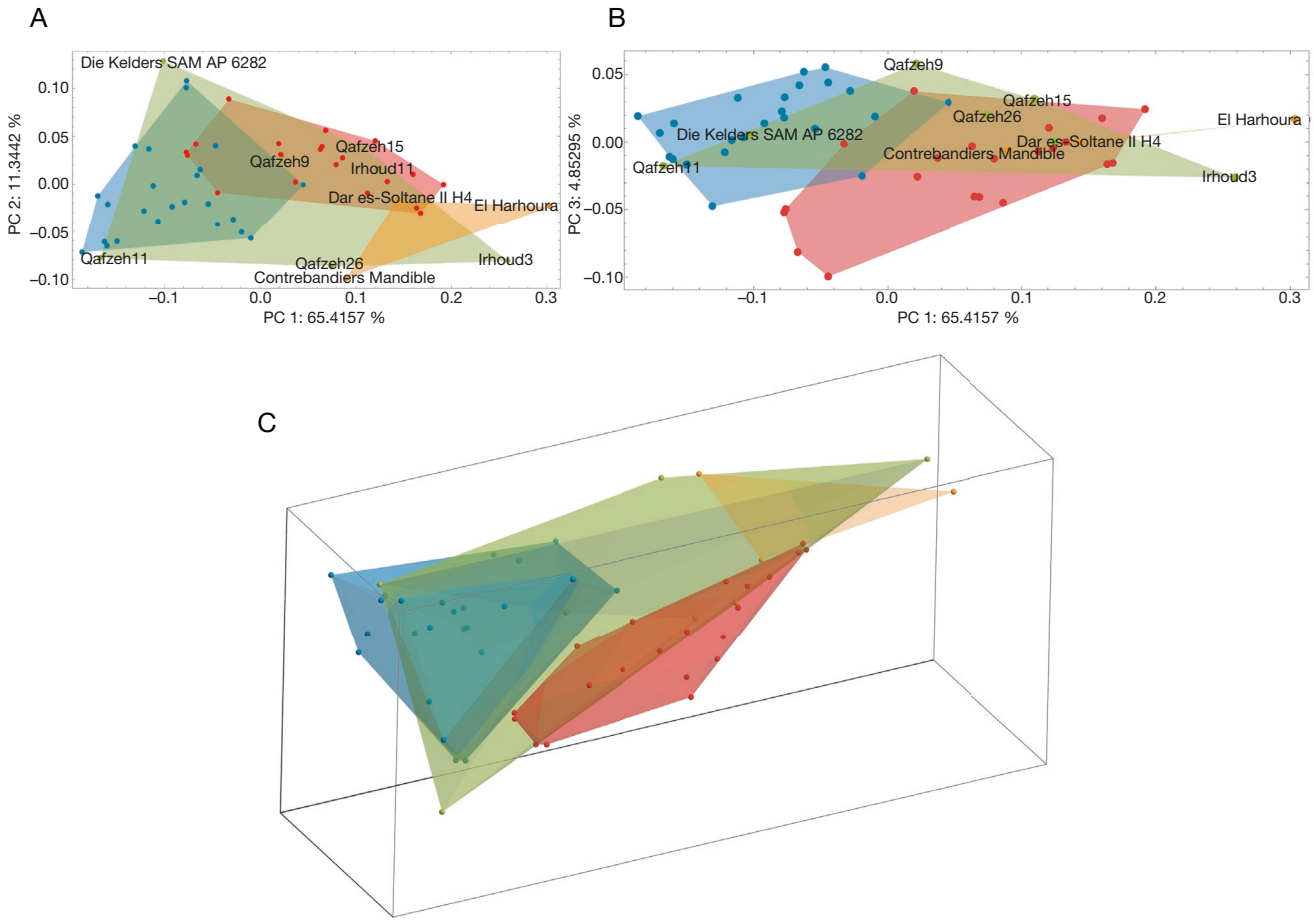

Fig. 9. — Principal component analysis (PCA) plots of enamel-dentine junction (EDJ) form the second mandibular molar across Aterian (**orange**), fossil *Homo sapiens* (**green**), *H. neanderthalensis* (**red**), and recent *H. sapiens* specimens (**blue**): **A**, second mandibular molars (LM2) EDJ form (PC1 vs PC2); **B**, LM2 EDJ form (PC1 vs PC3); **C**, LM2 EDJ shape form (PC1, PC2, and PC3).

and recent *H. sapiens*. Aterians accentuate the expansion of the talonid crests seen in *H. sapiens* groups.

Another similarity between Aterians and both groups of *H. sapiens* is the placement of the metaconid. As noted by Martin *et al.* (2017), this cusp is more centrally positioned in *H. neanderthalensis*. In Figure 7A, the metaconid and protoconid horns of *H. neanderthalensis* appear more protruding and tilted toward the central basin than in recent and fossil *H. sapiens*. For this feature, Aterians align more closely with *H. sapiens*. A distinctive trait of the Aterian mean shape, however, is that all cusp horns – except the metaconid – are much lower than in both *H. sapiens* and *H. neanderthalensis*.

Principal component analysis of LM2 EDJ shape and form

Shape analysis of the LM2 EDJ is less discriminant in shape space than that of LM1 in separating the studied groups. Figure 8A shows the PCA plot of shape space (PC1 vs PC2), which explains 34.42% of variance on PC1 and 14.44% on PC2. Aterian specimens, including El Harhoura, Dar es-Soltane II H4, and Contrebandiers, are positioned almost entirely within the fossil *H. sapiens* distribution, with marginal overlap with *H. neanderthalensis* and recent *H. sapiens*. Dar es-Soltane II H4 is positioned at the limits of the distributions of recent *H. sapiens* and *H. neanderthalensis*. El Harhoura is the only individual well within the *H. neanderthalensis* distribution and outside the fossil and recent *H. sapiens* groups. Contrebandiers is positioned near the limit of the fossil *H. sapiens* variation.

Figure 8B shows the PCA plot of shape space (PC1 vs PC3), where PC1 explains 34.42% and PC3 explains 10.06% of variance. Aterians remain entirely within the variation of fossil *H. sapiens* but also overlap with *H. neanderthalensis* and recent *H. sapiens*. Contrebandiers aligns with the fossil *H. sapiens* and recent *H. sapiens* clusters, far from *H. neanderthalensis*. Dar es-Soltane II H4 retains a more primitive pattern closer to *H. neanderthalensis*. The PC1 vs PC3 shape space plot illustrates the Aterian position within a complex evolutionary framework. El Harhoura and Contrebandiers show stronger affinities with fossil and recent *H. sapiens*. Dar es-Soltane II H4 retains more *H. neanderthalensis*-like traits.

The distribution of specimens in a 3D shape space (PC1, PC2, and PC3) (Fig. 8C) highlights distinctions between recent *H. sapiens* and *H. neanderthalensis*, *H. neanderthalensis* are discriminated from recent *H. sapiens*. Fossil *H. sapiens* and Aterians plot in the intermediate domain of overlap between these poles.

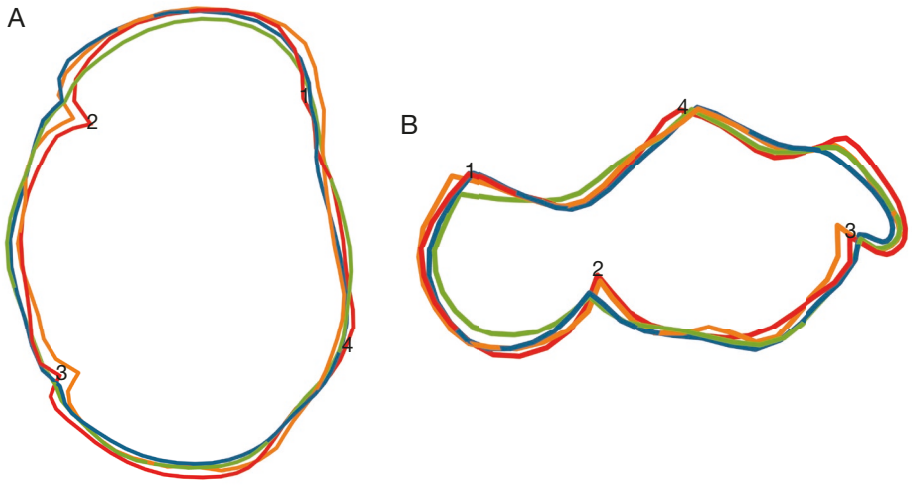

FIG. 10. — Between taxa comparisons of mean enamel-dentine junction (EDJ) shape of second mandibular molars: **A**, second mandibular molars (LM2) occlusal view; **B**, LM2 lateral view, across Aterians (**orange**), fossil *Homo sapiens* (**green**), *H. neanderthalensis* (**red**), and recent *H. sapiens* (**blue**). Key landmarks: **1**, protoconid; **2**, metaconid; **3**, entoconid; **4**, hypoconid.

Figure 9A shows PC1 vs PC2 in form space, with PC1 explaining 65.42% of the variance and PC2 explaining 11.34% of the variance. The distribution of Aterian specimens (El Harhoura, Dar es-Soltane II H4, and Contrebandiers) reveals a distinction in overall form compared to fossil *H. sapiens*, *H. neanderthalensis*, and recent *H. sapiens*. Fossil *H. sapiens* display very large shape variation, encompassing most of the variation observed in other groups and bridging the smaller recent *H. sapiens* and Aterians. *Homo neanderthalensis* displays reduced variation compared to fossil *H. sapiens*, but also occupies an intermediate position between Aterians and recent *H. sapiens*.

Figure 9B shows PC1 vs PC3 in form space, with PC1 explaining 65.42% of the variance and PC3 explaining 4.85% of the variance. Similar patterns to those observed in LM1 are evident. El Harhoura displays an extreme positioning along PC1, placing it far from the recent *H. sapiens* hull. Recent and fossil *H. sapiens* largely overlap along PC1 but do not separate significantly along PC2 or PC3, emphasizing the reduction in size in modern populations.

The 3D representation of the shape form space (PC1, PC2, and PC3) (Fig. 9C) highlights the morphological continuum between recent *H. sapiens*, fossil *H. sapiens*, and Aterians. *Homo neanderthalensis* individuals cluster tightly, exhibiting a well-defined form space. Fossil *H. sapiens* display greater variability, reflecting their wider geographical and temporal range. Recent *H. sapiens*, fossil *H. sapiens*, and Aterians range by increasing size along PC1, exhibiting larger size variability than *H. neanderthalensis*. This 3D plot shows a better separation of *H. neanderthalensis* from other groups, with less overlap compared to the LM1 EDJ analysis.

The EDJ contours of LM2 show less clear distinctions in their overall morphology compared to LM1 (Fig. 10C, D). Some of the distinctive features of each group observed in LM1 are still present, although less pronounced.

The difference in elongation of the crest outline between Aterians and other groups is barely visible. However, the more central positioning of the metaconid and the shortening of the spacing between the metaconid and protoconid in *H. neanderthalensis* remain evident. Aterians display an incipient tilt of the metaconid, along with a more central positioning of the entoconid, similar to *H. neanderthalensis*.

In general, across all groups, except for the metaconid in Aterians and *H. neanderthalensis* and the entoconid in Aterians, the occlusal projection of the horns relative to the crests is weaker than that observed in LM1.

DISCUSSION AND CONCLUSION

As previously concluded by other studies (e.g., Martin *et al.* 2017), *H. neanderthalensis* EDJ displays several distinctive features that separate them from *H. sapiens*, a finding fully confirmed by our study. When considered separately in the shape and form analysis of the EDJ, the Aterian sample tends to group with fossil *H. sapiens* and not with *H. neanderthalensis*. However, it also displays distinctive features.

In general, LM1 displays more discriminative features than LM2 in separating these groups. One of the most striking features is the very large size of the molars, with centroid size values of Aterian teeth statistically higher than those of all other groups for LM1. For LM2, the differences in centroid size between Aterians and fossil *H. sapiens*, as well as between Aterians and *H. neanderthalensis*, are not statistically significant. Still, the median values of Aterian molars remain higher than in all other groups, and the lack of statistical significance likely results from the small size of our Aterian sample.

In terms of shape and form, when compared with recent and fossil *H. sapiens*, Aterians seem to represent an extreme in size within the species' variability. Differences in morphology might partly result from their older age and large size. This age may explain the occurrence of some primitive retentions, such as the more elongated outline of the basin surrounded by the EDJ crests of LM1, which is also present to a lesser extent in *H. neanderthalensis* and fossil

H. sapiens. For the largest individuals, such as El Harhoura, the form analyses clearly place them at the extremity of fossil *H. sapiens* variations. However, the same reasons may place these specimens within the *H. neanderthalensis* distribution in some shape analyses (e.g., PC1-PC2 shape space of LM2 EDJ, Fig. 8A).

Although the Aterian can be seen as a northwestern African representative of early *H. sapiens*, they still display unique features in addition to their extremely large size. Examples include the tilt and more centrally placed LM2 entoconid horn of the EDJ and the lower protrusion of the LM1 horns (except for the metaconid). These features are not observed in other groups.

Recent *H. sapiens* display a significant reduction in size compared to fossil *H. sapiens*, accompanied by some level of morphological simplification. The Klasies River site provides an informative comparison for understanding the broader trajectory of dental evolution in MSA populations toward Recent *H. sapiens* patterns. As documented by Grine *et al.* (2021), the molars from Klasies River exhibit marked cusp reduction and occlusal flattening, with significant height reduction. The protoconid, metaconid, and hypoconid of the Klasies River molars are consistently reduced in height and display smooth occlusal surfaces. The hypoconid and entoconid are particularly flattened compared to the elevated cusps seen in *H. neanderthalensis* and Aterians.

Interestingly, while Klasies River molars show dental simplification earlier than other populations, they also exhibit notable variability, including pronounced differences in EDJ characteristics. These patterns mirror the diversity observed in Aterian specimens, which share robust EDJ features but also display unique features.

It remains to explain why the Aterians, displayed larger dentition compared to penecontemporaneous groups, including *H. neanderthalensis* and other fossil *H. sapiens*. One potential explanation could involve some degree of isolation relative to other African and southwestern Asian groups of early *H. sapiens.* This isolation, combined with local adaptation, could have contributed to the observed large variability within fossil *H. sapiens*. Limited gene flow between these groups may have promoted evolutionary divergence resulting from episodes of genetic drift.

The period of the Aterian technocomplex is characterized by increasing aridity in North Africa. Aterian toolmakers are sometimes described as "desert-adapted". Toward the end of their chronological range, the density of Aterian sites declined in Sahara, with the last populations surviving in oases and coastal areas (Garcea 2012). The dental remains analyzed in this study derive exclusively from Moroccan coastal sites, which eventually represented one of the last refugia of Aterian populations.

The comparative analysis of EDJ morphology in both LM1 and LM2 sheds light on the evolutionary trajectory of Aterians, an enigmatic population from the MSA of northwestern Africa. The distinctiveness of Aterian EDJ morphology reinforces their evolutionary separation from *H. neanderthalensis* and recent *H. sapiens*. This distinctiveness illustrates the mosaic nature of hominin evolution during the Middle to Late Pleistocene and the diversity of fossil *H. sapiens* African and southwestern Asian populations.

Future research, incorporating broader comparative material, will be essential to further elucidate the evolutionary relationships between Aterians, other fossil *H. sapiens*, and *H. neanderthalensis*. Such studies will contribute to a deeper understanding of hominin diversity during the Middle to Late Pleistocene.

Acknowledgements

We are especially grateful for the scanning assistance provided by Mathew Skinner, Heiko Temming, Kornelius Kupczik, Tanya Smith, and Adeline Le Cabec, whose contributions were essential to the success of this study. We extend our sincere gratitude to Mathew Skinner and Zeljko Rezek for their insightful discussions and invaluable advice throughout this research. Special thanks are owed to Lukas Westphal, David Plotzki, and Heiko Temming from the Max Planck Institute for Evolutionary Anthropology (MPI-EVA) for their exceptional technical support during the acquisition and segmentation of the micro-CT scans. We are also grateful to the Institut National des Sciences de l'Archéologie et du Patrimoine, as well as the dedicated staff of their library, for their continued assistance. We deeply appreciate the access to crucial specimens, generously provided by Antonio Rosas (Museo Nacional de Ciencias Naturales), Flora Groening (Senckenberg, Forschungsstation für Quartärpaläontologie), Roberto Macchiarelli (The *H. neanderthalensis* Tools Project), Michel Toussaint (ASBL Archéologie Andennaise, Royal Belgian Institute of Natural Sciences), Jakov Radovčić (Croatian Natural History Museum), Dejana Brajković (Croatian Academy of Sciences and Arts), Jean-Jacques Cleyet-Merle (Musée National de la Préhistoire des Eyzies-de-Tayac), Yoel Rak, Alon Barash, Israel Hershkovitz (Sackler School of Medicine, Tel Aviv University), Jean-François Tournepiche (Musée d'Angoulême), Almut Hoffmann (Museum für Vor- und Frühgeschichte Berlin), Don Reid (personal collection of clinical dental extractions, MPI-EVA), Andrei Dorian Soficaru ("Francisc J. Rainer" Institute of Anthropology), and Christine Feja (Leipzig University, Institut für Anatomie). We also thanks the editor-in-chief of the journal *Comptes Rendus Palevol*, Michel Laurin, the associate editor, Aurélien Mounier, and the reviewers.

REFERENCES

Aumassip G. 2004. — *Préhistoire du Sahara et de ses abords. Tome 1. Au temps des chasseurs : le Paléolothique*. Maisonneuve & Larose, Paris, 300 p.

Bailey S. 2006. — Beyond shovel-shaped incisors: Neandertal dental morphology in a comparative context. *Periodicum biologorum* 108 (3): 253-267.

Bailey S. E., Skinner M. M. & Hublin J.-J. 2011. — What lies beneath? An evaluation of lower molar trigonid crest patterns based on both dentine and enamel expression. *American Journal of Physical Anthropology* 145 (4): 505-518. https://doi.org/10.1002/ajpa.21468

Balout L. A. 1955. — *Préhistoire de l'Afrique du Nord : essai de chronologie*. Arts et métiers graphiques, Paris, 543 p.

Barton R. N. E., Bouzouggar A., Collcutt S. N., Schwenninger J.-L. & Clark-Balzan L. 2009. — OSL dating of the Aterian levels at Dar es-Soltan I (Rabat, Morocco) and implications for the dispersal of modern *Homo sapiens*. *Quaternary Science Reviews* 28 (19-20): 1914-1931. https://doi.org/10.1016/j.quascirev.2009.03.010

Bergmann I., Hublin J.-J., Ben-Ncer A., Sbihi-Alaoui F., Gunz P. & Freidline S. 2022. — The relevance of late MSA mandibles on the emergence of modern morphology in Northern Africa. *Scientific Reports* 12: 8841. https://doi.org/10.1038/s41598-022-12607-5

Bermúdez de Castro J. M., Rosas A., Carbonell E., Nicolás M. E., Rodríguez J. & Arsuaga J. L. 1999. — A modern human pattern of dental development in Lower Pleistocene hominids from Atapuerca-TD6 (Spain). *Proceedings of the National Academy of Sciences* 96 (7): 4210-4213. https://doi.org/10.1073/pnas.96.7.4210

Bouzouggar A., Barton N., Vanhaeren M., d'Errico F., Collcutt S., Higham T., Hodge E., Parfitt S., Rhodes E., Schwenninger J.-L., Stringer C., Turner E., Ward S., Moutmir A. & Stambouli A. 2007. — 82,000-year-old shell beads from North Africa and implications for the origins of modern human behavior. *Proceedings of the National Academy of Sciences* 104 (24): 9964-9969. https://doi.org/10.1073/pnas.0703877104

Bouzouggar A., Humphrey L. T., Barton N., Parfitt S. A., Balzan L. C., Schwenninger J.-L., Hajraoui M. A. E., Nespoulet R. & Bello S. M. 2018. — 90,000 year-old specialised bone technology in the Aterian Middle Stone Age of North Africa. *PLOS ONE* 13: e0202021. https://doi.org/10.1371/journal.pone.0202021

Braga J., Thackeray J. F., Subsol G., Kahn J. L., Maret D., Treil J. & Beck A. 2010. — The enamel–dentine junction in the postcanine dentition of *Australopithecus africanus*: intra-individual metameric and antimeric variation. *Journal of Anatomy* 216 (1): 62-79. https://doi.org/10.1111/j.1469-7580.2009.01154.x

Butler P. M. 1956. — The ontogeny of molar pattern. *Biological Reviews* 31 (1): 30-69. https://doi.org/10.1111/j.1469-185X.1956.tb01551.x

Cavanhié N. 2011. — L'ours qui a vu l'homme ? Étude archéozoologique et taphonomique du site paléolithique moyen de Regourdou (Montignac, Dordogne, France). *PALEO. Revue d'archéologie préhistorique* 21: 39-63. https://doi.org/10.4000/paleo.1742

Corruccini R. S. 1987. — The dentinoenamel junction in primates. *International Journal of Primatology* 8: 99-114. https://doi.org/10.1007/BF02735159

Corruccini R. S. 1998. — *The dentino-enamel junction in primate mandibular molars. Human Dental Development, Morphology, and Pathology: A Tribute to Albert A. Dahlberg*. University of Oregon Anthropological Papers, Portland: 1-16.

d'Errico F., Vanhaeren M., Barton N., Bouzouggar A., Mienis H., Richter D., Hublin J.-J., McPherron S. P. & Lozouet P. 2009. — Additional evidence on the use of personal ornaments in the Middle Paleolithic of North Africa. *Proceedings of the National Academy of Sciences* 106 (38): 16051-16056. https://doi.org/10.1073/pnas.0903532106

Debénath A. 1976. — La Grotte de Dar-es-Soltane II à Rabat (Maroc). Géologie et préhistoire. *Bulletins et Mémoires de la Société d'Anthropologie de Paris* 3 (2): 181-182. https://doi.org/10.3406/bmsap.1976.1848

Debénath A. 1980. — Nouveaux restes humains atériens du Maroc. *Comptes Rendus de l'Académie des Sciences* 290: 851-852.

Debénath A., Raynal J.-P., Roche J., Texier J. P. & Ferembach D. 1986. — Stratigraphie, habitat, typologie et devenir de l'Atérien marocain : données récentes. *L'Anthropologie* 90: 233-246.

Delpech F. 1996. — L'environnement animal des Moustériens Quina du Périgord. *Paléo, Revue d'Archéologie Préhistorique* 8: 31-46. https://doi.org/10.3406/pal.1996.905

Dibble H. L., Reed D., Rezek Z., Richter D., Roberts R. G., Sandgathe D., Schurmans U., Skinner A. R., Steele T. E. & Reed K. 2012. — New excavations at the site of Contrebandiers Cave, Morocco. *PaleoAnthropology* 2012: 145-201.

Ding H., Cui Z., Maghami E., Chen Y., Matinlinna J. P., Pow E. H. N., Fok A. S. L., Burrow M. F., Wang W. & Tsoi J. K. H. 2023. — Morphology and mechanical performance of dental crown designed by 3D-DCGAN. *Dental materials* 39 (3): 320-332. https://doi.org/10.1016/j.dental.2023.02.001

El Hajraoui M. A. 1994. — L'industrie osseuse atérienne de la grotte d'El Mnasra (Région de Témara, Maroc). *Préhistoire, anthropologie méditerranéennes* 3: 91-94.

El Hajraoui M. A., Oudouche H. & Nespoulet R. 2012. — Étude des coquilles perforées découvertes á Témara, *in* El Hajraoui A. M., Nespoulet R., Debénath A. & Dibble H. L. (dirs), *Préhistoire de la région de Rabat-Témara*. Presented at the Préhistoire de la région de Rabat-Témara, Institut National des Sciences de l'Archéologie et du Patrimoine, Rabat: 191-199.

El Hajraoui M., Nespoulet R., Debénath A. & Dibble H. 2012. — La Préhistoire de la région de Rabat-Témara. Institut national des sciences de l'archéologie et du patrimoine (INSAP), Rabat, 300 p.

Ellwood B. B., Harrold F. B., Benoist S. L., Thacker P., Otte M., Bonjean D., Long G. J., Shahin A. M., Hermann R. P. & Grandjean F. 2004. — Magnetic susceptibility applied as an age–depth–climate relative dating technique using sediments from Scladina Cave, a Late Pleistocene cave site in Belgium. *Journal of Archaeological Science* 31 (3): 283-293. https://doi.org/10.1016/j.jas.2003.08.009

Ferembach D. 1976. — Les restes humains de la Grotte de Dar-es-Soltane II (Maroc). Campagne 1975. *Bulletins et Mémoires de la Société d'Anthropologie de Paris* 3 (2): 183-193. https://doi.org/10.3406/bmsap.1976.1849

Garcea E. A. A. 2012. — Successes and failures of human dispersals from North Africa. *Quaternary International* 270: 119-128. https://doi.org/10.1016/j.quaint.2011.06.034

Grine F. & Klein R. 1985. — Pleistocene and Holocene human remains from Equus Cave, South Africa. *Anthropology* 8: 55-98.

Grine F. E., Gonzalvo E., Rossouw L., Holt S., Black W. & Braga J. 2021. — Variation in Middle Stone Age mandibular molar enamel-dentine junction topography at Klasies River Main Site assessed by diffeomorphic surface matching. *Journal of Human Evolution* 161: 103079. https://doi.org/10.1016/j.jhevol.2021.103079

Guadelli J.-L. & Laville H. 1988. — L'environnement climatique de la fin du Moustérien à Combe Grenal et à Camiac. Confrontation des données naturalistes et implications, *in* Farizy C. (dir.), *Paléolithique Moyen Récent et Paléolithique Supérieur Ancien en Europe*. Colloque international de Nemours, 9-11 mai 1988. CNRS (Mémoires du Musée de Préhistoire d'Île-de-France; 3), Paris: 43-48.

Guérin G., Discamps E., Lahaye C., Mercier N., Guibert P., Turq A., Dibble H. L., McPherron S. P., Sandgathe D. & Goldberg P. 2012. — Multi-method (TL and OSL), multi-material (quartz and flint) dating of the Mousterian site of Roc de Marsal (Dordogne, France): correlating Neanderthal occupations with the climatic variability of MIS 5–3. *Journal of Archaeological Science* 39 (10): 3071-3084. https://doi.org/10.1016/j.jas.2012.04.047

Gunz P., Mitteroecker P. & Bookstein F. L. 2005. — Semilandmarks in Three Dimensions, *in* Slice D. E. (ed.), *Modern Morphometrics in Physical Anthropology, Developments in Primatology: Progress and Prospects*. Springer US, Boston, MA: 73-98. https://doi.org/10.1007/0-387-27614-9_3

Guy F., Gouvard F., Boistel R., Euriat A. & Lazzari V. 2013. — Prospective in (Primate) dental analysis through tooth 3D topographical quantification. *PLOS ONE* 8: e66142. https://doi.org/10.1371/journal.pone.0066142

Guy F., Lazzari V., Gilissen E. & Thiery G. 2015. — To what extent is primate second molar enamel occlusal morphology shaped by the enamel-dentine junction? *PLOS ONE* 10: e0138802. https://doi.org/10.1371/journal.pone.0138802

Harvati K. & Hublin J.-J. 2012. — Morphological continuity of the face in the Late Middle and Late Pleistocene Hominins from Northwestern Africa: a 3D geometric morphometric analysis, *in* Hublin J.-J. & McPherron S. P. (eds), *Modern Origins: A North African Perspective, Vertebrate Paleobiology and Paleoanthropology*. Springer Netherlands, Dordrecht: 179-188. https://doi.org/10.1007/978-94-007-2929-2_12

Hublin J.-J., Verna C., Bailey S., Smith T., Olejniczak A., Sbihi-Alaoui F. Z. & Zouak M. 2012. — Dental evidence from the Aterian Human populations of Morocco, *in* Hublin J.-J. & McPherron S. P. (eds), *Modern Origins*. Springer Netherlands, Dordrecht: 189-204. https://doi.org/10.1007/978-94-007-2929-2_13

Hublin J.-J., Ben-Ncer A., Bailey S. E., Freidline S. E., Neubauer S., Skinner M. M., Bergmann I., Le Cabec A., Benazzi S., Harvati K. & Gunz P. 2017. — New fossils from Jebel Irhoud, Morocco and the pan-African origin of *Homo sapiens*. *Nature* 546: 289-292. https://doi.org/10.1038/nature22336

Ichou F. Z. B. & Bouzouggar A. 2020. — Contribution à l'étude du MSA au Maroc : processus de fabrication et de traitement des matières colorantes. *Bulletin d'Archéologie Marocaine* 25: 15-32. https://doi.org/10.34874/IMIST.PRSM/bam-v25.29657

Jacobs Z., Meyer M. C., Roberts R. G., Aldeias V., Dibble H. & El Hajraoui M. A. 2011. — Single-grain OSL dating at La Grotte des Contrebandiers ('Smugglers' Cave'), Morocco: improved age constraints for the Middle Paleolithic levels. *Journal of Archaeological Science* 38 (12): 3631-3643. https://doi.org/10.1016/j.jas.2011.08.033

Jernvall J. & Jung H. S. 2000. — Genotype, phenotype, and developmental biology of molar tooth characters. *American Journal of Physical Anthropology* 113 (Supplement 31): 171-190. https://doi.org/10.1002/1096-8644(2000)43:31+<171::aid-ajpa6>3.0.co;2-3

Johanson D. C. & White T. D. 1979. — A systematic assessment of Early African Hominids. *Science* 203 (4378): 321-330. https://doi.org/10.1126/science.104384

Khalaf K., Elcock C., Smith R. N. & Brook A. H. 2005. — Fluctuating dental asymmetry of multiple crown variables measured by an image analysis system. *Archives of Oral Biology* 50 (2): 249-253. https://doi.org/10.1016/j.archoralbio.2004.08.013

Korenhof C. A. W. 1961. — The enamel-dentine border: a new morphological factor in the study of the (human) molar pattern. *Proceedings of the section of sciences: Koninklijke Akademie van Wetenschappen* 64: 639-664.

Korenhof C. 1982. — *A peculiar fin of human enamel caps by Von Koenigswald in the surroundings of Sangiran, Java, and its evolutionary significance*. Modern Quaternary Research in Southeast Asia, Rotterdam: 227-236.

Macchiarelli R., Bondioli L., Debénath A., Mazurier A., Tournepiche J.-F., Birch W. & Dean M. C. 2006. — How Neanderthal molar teeth grew. *Nature* 444: 748-751. https://doi.org/10.1038/nature05314

Martin H. 1920. — Présentation d'un crâne d'enfant de 8 ans trouvé en place dans le mousterien de La Quina (Charente). *Bulletins et Mémoires de la Société d'Anthropologie de Paris* 1: 113-125.

Martin R. M. G., Hublin J.-J., Gunz P. & Skinner M. M. 2017. — The morphology of the enamel–dentine junction in Neanderthal molars: gross morphology, non-metric traits, and temporal trends. *Journal of Human Evolution* 103: 20-44. https://doi.org/10.1016/j.jhevol.2016.12.004

Martínez de Pinillos M., Martinón-Torres M., Skinner M. M., Arsuaga J. L., Gracia-Téllez A., Martínez I., Martín-Francés L. & Bermúdez de Castro J. M. 2014. — Trigonid crests expression in Atapuerca-Sima de los Huesos lower molars: Internal and external morphological expression and evolutionary inferences. *Comptes Rendus Palevol* 13 (3): 205-221. https://doi.org/10.1016/j.crpv.2013.10.008

Martinón-Torres M., Bermúdez de Castro J. M., Gómez-Robles A., Prado-Simón L. & Arsuaga J. L. 2012. — Morphological description and comparison of the dental remains from Atapuerca-Sima de los Huesos site (Spain). *Journal of Human Evolution* 62 (1): 7-58. https://doi.org/10.1016/j.jhevol.2011.08.007

Martinón-Torres M., Martínez de Pinillos M., Skinner M. M., Martín-Francés L., Gracia-Téllez A., Martínez I., Arsuaga J. L. & Bermúdez de Castro J. M. 2014. — Talonid crests expression at the enamel-dentine junction of hominin lower permanent and deciduous molars. *Comptes Rendus Palevol* 13 (3): 223-234. https://doi.org/10.1016/j.crpv.2013.12.002

Mellars P. & Grün R. 1991. — A comparison of the electron spin resonance and thermoluminescence dating methods: the results of ESR dating at Le Moustier (France). *Cambridge Archaeological Journal* 1: 269-276.

Ménard J. 1998. — Odontologie des dents de la grotte de Témara (Maroc). *Bulletin d'Archéologie Marocaine* 18: 67-97.

Ménard J. 2002. — Étude odontologique des restes aériens de Dar-Es-Soltane II et d'El-Harhoura II au Maroc. *Bulletin d'Archéologie Marocaine* 19: 67-118.

Mercier N. 1992. — *Apport des méthodes de datation radionucléaires à l'étude du peuplement préhistorique de l'Europe et du Proche-Orient au cours du Pléistocène supérieur*. Doctorat de l'Université de Bordeaux I, Bordeaux, 139 p.

Mercier N. & Valladas H. 1998. — Datations. *Gallia Préhistoire* 40: 70-71.

Mercier N., Valladas H., Bar-Yosef O., Vandermeersch B., Stringer C. & Joron J.-L. 1993. — Thermoluminescence date for the Mousterian burial site of Es-Skhul, Mt. Carmel. *Journal of Archaeological Science* 20 (2): 169-174. https://doi.org/10.1006/jasc.1993.1012

Minugh-Purvis N. 1993. — Reexamination of the immature hominid maxilla from Tangier, Morocco. *American Journal of Physical Anthropology* 92 (4): 449-61. https://doi.org/10.1002/ajpa.1330920404

Mitteroecker P. & Gunz P. 2013. — Semilandmarks: a method for quantifying curves and surfaces. *Hystrix* 24 (1): 103-109. https://doi.org/10.4404/hystrix-24.1-6292

Mitteroecker P., Gunz P., Windhager S. & Schaefer K. 2013. — A brief review of shape, form, and allometry in geometric morphometrics, with applications to human facial morphology. *Hystrix* 24 (1): 59. https://doi.org/10.4404/hystrix-24.1-6369

Morel J. 1974. — La station eponyme de l'Oued Djebbana à Bir-El-Ater (Est Algerien). Contribution à la connaissance de son industrie et de sa faune. La station éponyme de l'Oued Djebbana à Bir-El-Ater (Est Algerien). *Contribution à la connaissance de son industrie et de sa faune* 78: 53-80.

Morel J. & Le Bretagne A. 1978. — L'industrie atérienne de l'Oued Djouf El Djemel. Comparaison avec l'industrie de l'Oued Djebbana. Le complexe atérien du Maghreb Oriental. *Bulletin de la Société préhistorique française* 75: 487-500.

Morita W., Yano W., Nagaoka T., Abe M., Ohshima H. & Nakatsukasa M. 2014. — Patterns of morphological variation in enamel-dentin junction and outer enamel surface of human molars. *Journal of Anatomy* 224 (6): 669-680. https://doi.org/10.1111/joa.12180

Napolitano R., Alichane H., Martini P., Di Domenico G., Martin R. M., Hublin J. J. & Oxilia G. 2026. — A machine learning pipeline for cusp height prediction in worn lower

molars: methodological proof-of-concept and validation across *Homo*. *Applied Sciences* 16 (3): 1280. https://doi.org/10.3390/app16031280

Nespoulet R. & El Hajraoui M. A. 2012. — Présentation du site et archéostratigraphies, *in* El Hajraoui A. M., Nespoulet R., Debénath A. & Dibble H. L. (dirs), *Préhistoire de la région de Rabat-Témara*. Presented at the Préhistoire de la région de Rabat-Témara, Institut National des Sciences de l'Archéologie et du Patrimoine, Rabat: 27-30.

Ortiz A., Skinner M. M., Bailey S. E. & Hublin J.-J. 2012. — Carabelli's trait revisited: an examination of mesiolingual features at the enamel–dentine junction and enamel surface of *Pan* and *Homo sapiens* upper molars. *Journal of Human Evolution* 63 (4): 586-596. https://doi.org/10.1016/j.jhevol.2012.06.003

Ortiz A., Bailey S. E., Hublin J.-J. & Skinner M. M. 2017. — Homology, homoplasy and cusp variability at the enamel-dentine junction of hominoid molars. *Journal of Anatomy* 231 (4): 585-599. https://doi.org/10.1111/joa.12649

Oxilia G., Bortolini E., Martini S., Papini A., Boggioni M., Buti L., Figus C., Sorrentino R., Townsend G. & Kaidonis J. 2018. — The physiological linkage between molar inclination and dental macrowear pattern. *American Journal of Physical Anthropology* 166 (4): 941-951. https://doi.org/10.1002/ajpa.23476

Oxilia G., Zaniboni M., Bortolini E., Sartorio J. C. M., Bernardini F., Tuniz C., Di Domenico G., Pavičić D. T., Los D. & Radović S. 2023. — Enamel thickness per masticatory phases (ETMP): A new approach to assess the relationship between macrowear and enamel thickness in the human lower first molar. *Journal of archaeological science* 153: 105776. https://doi.org/10.1016/j.jas.2023.105776

Oxilia G., Tomasella M. & Cecere A. 2025. — Dental morphology in restorative dentistry: a pilot study on morphological consistency and variability in human upper first molars. *Dentistry Journal* 13 (3): 122. https://doi.org/10.3390/dj13030122

Pirson S., Bonjean D. & Toussaint M. 2014. — *Stratigraphic origin of the juvenile remains from Scladina cave: re-evaluation and consequences for their palaeoenvironmental and chronostratigraphic contexts. The Scladina I-4A Juvenile Neandertal (Andenne, Belgium): Palaeoanthropology and Context*. Études et Recherches Archéologiques de Université de Liège, Liège: 93-124.

Raynal J.-P. & Occhietti S. 2012. — Amino Chronology and an Earlier Age for the Moroccan Aterian, *in* Hublin J.-J. & McPherron S. P. (eds), *Modern Origins: A North African Perspective, Vertebrate Paleobiology and Paleoanthropology*. Springer Netherlands, Dordrecht: 79-90. https://doi.org/10.1007/978-94-007-2929-2_6

Richter D., Moser J., Nami M., Eiwanger J. & Mikdad A. 2010. — New chronometric data from Ifri n'Ammar (Morocco) and the chronostratigraphy of the Middle Palaeolithic in the Western Maghreb. *Journal of Human Evolution* 59 (6): 672-679. https://doi.org/10.1016/j.jhevol.2010.07.024

Richter D., Grün R., Joannes-Boyau R., Steele T. E., Amani F., Rué M., Fernandes P., Raynal J.-P., Geraads D., Ben-Ncer A., Hublin J.-J. & McPherron S. P. 2017. — The age of the hominin fossils from Jebel Irhoud, Morocco, and the origins of the Middle Stone Age. *Nature* 546: 293-296. https://doi.org/10.1038/nature22335

Rink W. J., Schwarcz H. P., Smith F. H. & Radovčić J. 1995. — ESR ages for Krapina hominids. *Nature* 378: 24-24. https://doi.org/10.1038/378024a0

Robinson J. T. 1956. — The dentition of the Australopithecinae: Australopithecines and hominid phylogenesis. *Transvaal Museum Memoirs* 9 (1): 158-175. https://hdl.handle.net/10520/AJA0000012_159

Roche J. 1976. — Chronostratigraphie des restes atériens de la Grotte des Contrebandiers à Témara (Province de Rabat). *Bulletins et Mémoires de la Société d'Anthropologie de Paris* 3: 165-173. https://doi.org/10.3406/bmsap.1976.1846

Roche J. & Texier J.-P. 1976. — Découverte de restes humains dans un niveau atérien supérieur de la grotte des Contrebandiers, à Temara (Maroc). *Comptes Rendus de l'Académie des Sciences, Paris* 282: 45-47.

Röding C., Stringer C., Lacruz R. & Harvati K. 2022. — Mugharet el'Aliya: affinities of an enigmatic north African Aterian maxillary fragment. *American Journal of Biological Anthropology* 180. https://doi.org/10.1002/ajpa.24642

Rohlf F. J. & Slice D. 1990. — Extensions of the Procrustes Method for the optimal superimposition of landmarks. *Systematic Biology* 39: 40-59. https://doi.org/10.2307/2992207

Romandini M., Oxilia G., Bortolini E., Peyrégne S., Delpiano D., Nava A., Panetta D., Di Domenico G., Martini P. & Arrighi S. 2020. — A late Neanderthal tooth from north-eastern Italy. *Journal of Human Evolution* 147: 102867. https://doi.org/10.1016/j.jhevol.2020.102867

Schwarcz H. P. & Rink W. J. 2000. — ESR dating of the Die Kelders Cave 1 site, South Africa. *Journal of Human Evolution* 38 (1): 121-128. https://doi.org/10.1006/jhev.1999.0352

Schwenninger J., Collcutt S., Barton N., Bouzouggar A., Clark-Balzan L., Hajraoui M., Nespoulet R. & Debénath A. 2010. — A new luminescence chronology for Aterian cave sites on the Atlantic Coast of Morocco, *in* Garcea E. A. A. (ed.), *South-Eastern Mediterranean Peoples between 130,000 and 10,000 Years Ago*. Oxbow books, Oxford: 18-36.

Sehasseh E. M., Fernandez P., Kuhn S., Stiner M., Mentzer S., Colarossi D., Clark A., Lanoe F., Pailes M., Hoffmann D., Benson A., Rhodes E., Benmansour M., Laissaoui A., Ziani I., Vidal-Matutano P., Morales J., Djellal Y., Longet B., Hublin J.-J., Mouhiddine M., Rafi F.-Z., Worthey K. B., Sanchez-Morales I., Ghayati N. & Bouzouggar A. 2021. — Early Middle Stone Age personal ornaments from Bizmoune Cave, Essaouira, Morocco. *Science Advances* 7 (39): eabi8620. https://doi.org/10.1126/sciadv.abi8620

Şenyürek M. S. 1940. — *Fossil Man in Tangier*. Peabody Museum Press, Cambridge, Massachusetts, 46 p.

Skinner M. 2008. — *Enamel-dentine junction morphology of extant hominoid and fossil hominin lower molars*. PhD George Washington University, 202 p.

Skinner M. M. & Gunz P. 2010. — The presence of accessory cusps in chimpanzee lower molars is consistent with a patterning cascade model of development. *Journal of Anatomy* 217 (3): 245-253. https://doi.org/10.1111/j.1469-7580.2010.01265.x

Skinner M. M., Gunz P., Wood B. A. & Hublin J.-J. 2008a. — Enamel-dentine junction (EDJ) morphology distinguishes the lower molars of *Australopithecus africanus* and *Paranthropus robustus*. *Journal of Human Evolution* 55 (6): 979-988. https://doi.org/10.1016/j.jhevol.2008.08.013

Skinner M. M., Wood B. A., Boesch C., Olejniczak A. J., Rosas A., Smith T. M. & Hublin J.-J. 2008b. — Dental trait expression at the enamel-dentine junction of lower molars in extant and fossil hominoids. *Journal of Human Evolution* 54 (2): 173-186. https://doi.org/10.1016/j.jhevol.2007.09.012

Skinner M. M., Gunz P., Wood B. A., Boesch C. & Hublin J.-J. 2009a. — Discrimination of extant *Pan* species and subspecies using the enamel-dentine junction morphology of lower molars. *American Journal of Physical Anthropology* 140 (2): 234-243. https://doi.org/10.1002/ajpa.21057

Skinner M. M., Gunz P., Wood B. A. & Hublin J.-J. 2009b. — How many landmarks? Assessing the classification accuracy of Pan lower molars using a geometric morphometric analysis of the occlusal basin as seen at the enamel-dentine junction. *Frontiers of Oral Biology* 13: 23-29. https://doi.org/10.1159/000242385

Skinner M. M., Wood B. A. & Hublin J.-J. 2009c. — Protostylid expression at the enamel-dentine junction and enamel surface of mandibular molars of *Paranthropus robustus* and *Australopithecus africanus*. *Journal of Human Evolution* 56 (1): 76-85. https://doi.org/10.1016/j.jhevol.2008.08.021

Skinner M. M., Evans A., Smith T., Jernvall J., Tafforeau P., Kupczik K., Olejniczak A. J., Rosas A., Radovčič J., Thackeray J. F., Toussaint M. & Hublin J.-J. 2010. — Brief communication: Contributions of enamel-dentine junction shape and enamel deposition to primate molar crown complexity. *American Journal of Physical Anthropology* 142 (1): 157-163. https://doi.org/10.1002/ajpa.21248

Steele T. E., Álvarez-Fernandez E. & Hallett-Desguez E. 2019. — Early personal ornaments --- A review of shells as personal ornamentation during the African Middle Stone Age. *PaleoAnthropology* 2019: 24-51. https://doi.org/10.4207/PA.2019.ART122

Suwa G., Wood B. A. & White T. D. 1994. — Further analysis of mandibular molar crown and cusp areas in Pliocene and early Pleistocene hominids. *American Journal of Physical Anthropology* 93 (4): 407-426. https://doi.org/10.1002/ajpa.1330930402

Teilhol V. 2002. — Contribution à l'étude individuelle des ossements d'enfants de la-Chaise-de-Vouthon (Charente, France) : approche paléodémographique, paléolithnologique, aspect morphologique et étude métrique. Place phylogénique des enfants de la Chaise. *Bulletin de la Société préhistorique française* 99 (2): 382-384. https://www.jstor.org/stable/27924229

Thesleff I. 2000. — Genetic basis of tooth development and dental defects. *Acta Odontol Scand* 58 (5): 191-194. https://doi.org/10.1080/000163500750051728

Thesleff I. 2006. — The genetic basis of tooth development and dental defects. *American Journal of Medical Genetics Part A* 140a (23): 2530-2535. https://doi.org/10.1002/ajmg.a.31360

Tixier J. 1967. — *Pièces pédonculées atériennes du Maghreb et du Sahara : types 1-30*. Muséum national d'Histoire naturelle, Paris: 1-68.

Trinkaus E. 1978. — Dental remains from the Shanidar adult Neanderthals. *Journal of Human Evolution* 7 (5): 369-382. https://doi.org/10.1016/S0047-2484(78)80087-6

Turq A., Jaubert J., Maureille B. & Laville D. 2008. — *Le cas des sépultures néandertaliennes du Sud-Ouest : et si on les vieillissait? Première humanité, gestes funéraires des Néandertaliens*. Réunion des Musées Nationaux, Paris,: 40-41.

Valladas H., Geneste J. M., Joron J.-L. & Chadelle J. P. 1986. — Thermoluminescence dating of Le Moustier (Dordogne, France). *Nature* 322: 452-454. https://doi.org/10.1038/322452a0

Valladas H., Reyss J.-L., Joron J.-L., Valladas G., Bar-Yosef O. & Vandermeersch B. 1988. — Thermoluminescence dating of Mousterian Troto-Cro-Magnon'remains from Israel and the origin of modern man. *Nature* 331: 614-616. https://doi.org/10.1038/331614a0

Vallois H. V. & Roche J. 1958. — [The Acheulean mandible from Temara, Morocco]. *Comptes rendus hebdomadaires des séances de l'Académie des sciences* 246: 3113-3116.

Vandermeersch B. & Trinkaus E. 1995. — The postcranial remains of the Régourdou 1 Neandertal: the shoulder and arm remains. *Journal of Human Evolution* 28 (5): 439-476.

Vanhaereny M., d'Errico F., Stringer C., James S. L., Todd J. A. & Mienis H. K. 2006. — Middle Paleolithic shell beads in Israel and Algeria. *Science* 312 (5781): 1785-1788. https://doi.org/10.1126/science.1128139

Weidenreich F. 1937. — The dentition of *Sinanthropus pekinensis*: a comparative odontography of the hominids. *The national geological survey of China, Pall Sinica, n. s.* 0: 143-146.

Wild E. M., Paunovic M., Rabeder G., Steffan I. & Steier P. 2001. — Age determination of fossil bones from the Vindija Neanderthal site in Croatia. *Radiocarbon* 43: 1021-1028.

Wollny G., Kellman P., Ledesma-Carbayo M.-J., Skinner M. M., Hublin J.-J. & Hierl T. 2013. — MIA - A free and open source software for gray scale medical image analysis. *Source Code for Biology and Medicine* 8: 20. https://doi.org/10.1186/1751-0473-8-20

Wolpoff M. H. 1979. — The Krapina dental remains. *American Journal of Physical Anthropology* 50 (1): 67-113. https://doi.org/10.1002/ajpa.1330500110

Wood B. A., Abbott S. A. & Graham S. H. 1983. — Analysis of the dental morphology of Plio-Pleistocene hominids. II. Mandibular molars-study of cusp areas, fissure pattern and cross sectional shape of the crown. *Journal of Anatomy* 137 (Pt 2): 287-314.

Zanolli C. 2015. — Molar crown inner structural organization in Javanese *Homo erectus*. *American Journal of Physical Anthropology* 156 (1): 148-157. https://doi.org/10.1002/ajpa.22611

Zanolli C. & Mazurier A. 2013. — Endostructural characterization of the *H. heidelbergensis* dental remains from the early Middle Pleistocene site of Tighenif, Algeria. *Comptes Rendus Palevol* 12 (5): 293-304. https://doi.org/10.1016/j.crpv.2013.06.004

Zanolli C., Bondioli L., Mancini L., Mazurier A., Widianto H. & Macchiarelli R. 2012. — Brief communication: two human fossil deciduous molars from the sangiran dome (Java, Indonesia): outer and inner morphology. *American Journal of Physical Anthropology* 147 (3): 472-481. https://doi.org/10.1002/ajpa.21657

Zanolli C., Bondioli L., Coppa A., Dean C. M., Bayle P., Candilio F., Capuani S., Dreossi D., Fiore I., Frayer D. W., Libsekal Y., Mancini L., Rook L., Medin Tekle T., Tuniz C. & Macchiarelli R. 2014. — The late Early Pleistocene human dental remains from Uadi Aalad and Mulhuli-Amo (Buia), Eritrean Danakil: macromorphology and microstructure. *Journal of Human Evolution* 74: 96-113. https://doi.org/10.1016/j.jhevol.2014.04.005

Zanolli C., Grine F. E., Kullmer O., Schrenk F. & Macchiarelli R. 2015. — The early Pleistocene deciduous hominid molar FS-72 from the Sangiran dome of java, Indonesia: a taxonomic reappraisal based on its comparative endostructural characterization. *American Journal of Physical Anthropology* 157 (4): 666-674. https://doi.org/10.1002/ajpa.22748

Submitted on 12 February 2024;
accepted on 20 October 2025;
published on 18 March 2026.

APPENDICES

APPENDIX 1. — Centroid sizes of the first mandibular molars (LM1).

Specimens	Group	Tooth	Centroid size
Abri Suard 14-7	*H. neanderthalensis*	LM1	31.378
Abri Suard 49	*H. neanderthalensis*	LM1	33.055
Abri Suard 5	*H. neanderthalensis*	LM1	32.954
Combe-Grenal I	*H. neanderthalensis*	LM1	31.793
Combe-Grenal IV	*H. neanderthalensis*	LM1	33.189
Combe-Grenal 1048-69	*H. neanderthalensis*	LM1	31.186
Krapina 52	*H. neanderthalensis*	LM1	29.819
Krapina 53	*H. neanderthalensis*	LM1	35.378
Krapina 54	*H. neanderthalensis*	LM1	29.628
Krapina 55	*H. neanderthalensis*	LM1	35.572
Krapina 79	*H. neanderthalensis*	LM1	37.440
Krapina 81	*H. neanderthalensis*	LM1	31.651
Le Moustier	*H. neanderthalensis*	LM1	33.495
Roc de Marsal	*H. neanderthalensis*	LM1	32.724
Scladina A4A1	*H. neanderthalensis*	LM1	30.752
Scladina 756	*H. neanderthalensis*	LM1	33.293
Scladina 780	*H. neanderthalensis*	LM1	32.795
Combe-Grenal -I	*H. neanderthalensis*	LM1	31.761
Krapina 52	*H. neanderthalensis*	LM1	29.684
Krapina 53	*H. neanderthalensis*	LM1	35.040
Die Kelders SAM AP 6242	Fossil *H. sapiens*	LM1	32.213
Die Kelders SAM AP 6277	Fossil *H. sapiens*	LM1	32.286
Equus EQ H5	Fossil *H. sapiens*	LM1	32.221
Irhoud 3	Fossil *H. sapiens*	LM1	38.178
Qafzeh11	Fossil *H. sapiens*	LM1	27.824
Qafzeh15	Fossil *H. sapiens*	LM1	34.772
Qafzeh9	Fossil *H. sapiens*	LM1	34.130
Skhul1	Fossil *H. sapiens*	LM1	29.995
Contrebandiers Mandible T3a	Aterian	LM1	37.267
Dar es-Soltane II H4	Aterian	LM1	35.121
El Harhoura	Aterian	LM1	35.146
Contrebandiers Mandible	Aterian	LM1	39.071
Archaeological sites in Belgium Belgian 129a	Recent *H. sapiens*	LM1	28.641
Archaeological sites in Belgium Belgian 89a	Recent *H. sapiens*	LM1	30.422
Archaeological sites in Belgium Belgian 93a	Recent *H. sapiens*	LM1	32.197
Archaeological sites in Belgium Belgian A31	Recent *H. sapiens*	LM1	29.251
Archaeological sites in Belgium Belgian A32	Recent *H. sapiens*	LM1	30.803
Anatomical collections / Clinical extractions M161	Recent *H. sapiens*	LM1	29.304
Anatomical collections / Clinical extractions M3	Recent *H. sapiens*	LM1	28.971
Anatomical collections / Clinical extractions M5	Recent *H. sapiens*	LM1	29.603
Anatomical collections / Clinical extractions R1101-1498	Recent *H. sapiens*	LM1	29.916
Anatomical collections / Clinical extractions R1140-899	Recent *H. sapiens*	LM1	26.676
Anatomical collections / Clinical extractions R1160-440	Recent *H. sapiens*	LM1	29.775
Anatomical collections / Clinical extractions R123	Recent *H. sapiens*	LM1	28.466
Anatomical collections / Clinical extractions R167-I75	Recent *H. sapiens*	LM1	30.458
Anatomical collections / Clinical extractions R1989-1382	Recent *H. sapiens*	LM1	31.775
Anatomical collections / Clinical extractions R258-144	Recent *H. sapiens*	LM1	29.827
Anatomical collections / Clinical extractions R2602-1673	Recent *H. sapiens*	LM1	29.301
Anatomical collections / Clinical extractions R433	Recent *H. sapiens*	LM1	28.406
Anatomical collections / Clinical extractions R488-274	Recent *H. sapiens*	LM1	27.583
Anatomical collections / Clinical extractions R605-1185	Recent *H. sapiens*	LM1	26.784
Anatomical collections / Clinical extractions SI12	Recent *H. sapiens*	LM1	28.707
Anatomical collections / Clinical extractions ULAC-58	Recent *H. sapiens*	LM1	30.224
Anatomical collections / Clinical extractions ULAC-66	Recent *H. sapiens*	LM1	27.293
Anatomical collections / Clinical extractions ULAC-797	Recent *H. sapiens*	LM1	29.905

Appendix 2. — Centroid sizes of the second mandibular molars (LM2).

Specimens	Group	Tooth	Centroid size
Abri Suard S36	*H. neanderthalensis*	LM2	27.675
Krapina 105	*H. neanderthalensis*	LM2	35.197
Krapina 107	*H. neanderthalensis*	LM2	35.535
Krapina 1	*H. neanderthalensis*	LM2	36.267
Krapina 53	*H. neanderthalensis*	LM2	35.362
Krapina 54	*H. neanderthalensis*	LM2	28.605
Krapina 55	*H. neanderthalensis*	LM2	34.128
Krapina 57	*H. neanderthalensis*	LM2	33.473
Krapina 59	*H. neanderthalensis*	LM2	31.695
Krapina 6	*H. neanderthalensis*	LM2	31.062
Krapina 80	*H. neanderthalensis*	LM2	32.348
Krapina 86	*H. neanderthalensis*	LM2	32.411
Krapina 9	*H. neanderthalensis*	LM2	27.742
La Quina H9	*H. neanderthalensis*	LM2	31.676
Le Moustier	*H. neanderthalensis*	LM2	33.797
Regourdou	*H. neanderthalensis*	LM2	28.698
Scladina 4A1	*H. neanderthalensis*	LM2	30.374
Scladina 540	*H. neanderthalensis*	LM2	33.619
Scladina 755	*H. neanderthalensis*	LM2	31.647
Vindija Cave -11-39	*H. neanderthalensis*	LM2	30.536
Irhoud 11	Fossil *H. sapiens*	LM2	33.846
Irhoud 3	Fossil *H. sapiens*	LM2	38.977
Qafzeh 11	Fossil *H. sapiens*	LM2	25.835
Qafzeh 15	Fossil *H. sapiens*	LM2	33.502
Qafzeh 26	Fossil *H. sapiens*	LM2	32.901
Qafzeh 9	Fossil *H. sapiens*	LM2	30.957
Die Kelders SAM AP 6282	Fossil *H. sapiens*	LM2	26.583
Dar es-Soltane II H4	Aterian	LM2	34.665
El Harhoura	Aterian	LM2	40.377
Contrebandiers Mandible	Aterian	LM2	33.333
Archaeological sites in Belgium Belgian 13e	Recent *H. sapiens*	LM2	31.501
Anatomical collections / Clinical extractions M123	Recent *H. sapiens*	LM2	26.154
Anatomical collections / Clinical extractions M145	Recent *H. sapiens*	LM2	25.456
Anatomical collections / Clinical extractions M146	Recent *H. sapiens*	LM2	28.197
Anatomical collections / Clinical extractions M162	Recent *H. sapiens*	LM2	27.242
Anatomical collections / Clinical extractions M181	Recent *H. sapiens*	LM2	30.043
Anatomical collections / Clinical extractions M185	Recent *H. sapiens*	LM2	29.022
Anatomical collections / Clinical extractions M19	Recent *H. sapiens*	LM2	26.742
Anatomical collections / Clinical extractions M232	Recent *H. sapiens*	LM2	29.666
Anatomical collections / Clinical extractions M53	Recent *H. sapiens*	LM2	29.398
Anatomical collections / Clinical extractions M6	Recent *H. sapiens*	LM2	26.974
Anatomical collections / Clinical extractions R1101-1498	Recent *H. sapiens*	LM2	25.943
Anatomical collections / Clinical extractions R123	Recent *H. sapiens*	LM2	26.716
Anatomical collections / Clinical extractions R1639-1186	Recent *H. sapiens*	LM2	25.460
Anatomical collections / Clinical extractions R1719-1237	Recent *H. sapiens*	LM2	26.050
Anatomical collections / Clinical extractions R1989-1382	Recent *H. sapiens*	LM2	28.752
Anatomical collections / Clinical extractions R2070-1423	Recent *H. sapiens*	LM2	27.913
Anatomical collections / Clinical extractions R2207-1493	Recent *H. sapiens*	LM2	27.591
Anatomical collections / Clinical extractions R2525-1641	Recent *H. sapiens*	LM2	27.448
Anatomical collections / Clinical extractions R258-144	Recent *H. sapiens*	LM2	25.842
Anatomical collections / Clinical extractions R433	Recent *H. sapiens*	LM2	28.324
Anatomical collections / Clinical extractions R752-692	Recent *H. sapiens*	LM2	28.669
Anatomical collections / Clinical extractions ULAC-151	Recent *H. sapiens*	LM2	26.235
Anatomical collections / Clinical extractions ULAC-536	Recent *H. sapiens*	LM2	27.522